TECHNISCHE UNIVERSITÄT WIEN
Vienna University of Technology

Diplomarbeit

# Irradiation of Silicon detectors for HEP experiments in the Triga Mark II reactor of ATI

*zur Erlangung des akademischen Grades*

**Diplom-Ingenieur**

*im Rahmen des Studiums*

**Technische Physik**

*eingereicht von*

**Peter Salajka**
1125611

*ausgeführt am*

Atominstitut der TU Wien

*und am*

Institut für Hochenergiephysik der Österreichischen Akademie der Wissenschaften

*Betreuer*

**Privatdoz. Dipl.-Ing. Dr.techn. Christoph Schwanda**

*und*

**Univ.Lektor Dipl.-Ing. Dr.techn. Thomas Bergauer**

Wien, 23.08.2021

Verfasser | Betreuer

Die approbierte gedruckte Originalversion dieser Diplomarbeit ist an der TU Wien Bibliothek verfügbar
The approved original version of this thesis is available in print at TU Wien Bibliothek.
TU Bibliothek Your knowledge hub WIEN

Die approbierte gedruckte Originalversion dieser Diplomarbeit ist an der TU Wien Bibliothek verfügbar
The approved original version of this thesis is available in print at TU Wien Bibliothek.

# Zusammenfassung

Silizium ist aufgrund seiner Halbleitereigenschaften ein äußerst attraktives Material für Teilchendetektoren in der Hochenergiephysik (HEP). Eine kleine Bandlücke ermöglicht ein relativ großes Signal bei geringem Rauschen. Die Notwendigkeit der kryogenen Kühlung ist nicht gegeben. Die hohe Ladungsträgerbeweglichkeit impliziert hohe Detektorgeschwindigkeit. Einlaufende Teilchen erzeugen die Elektron-Loch-Paare, die für das Signal bei Drift im elektrischen Feld verantwortlich sind. Durch Strahlungsschädigung verschlechtert sich auch die Detektorleistung.

Dafür müssen sowohl mikroskopische Strahlungseffekte wie Punkt und Cluster Schäden des Einkristalls, als auch Kernreaktionen von Silizium Atomen, durch Messen von makroskopischen Parametern untersucht werden. Diese sind die Erhöhung des Dunkelstroms, die Änderung der vollen Verarmungsspannung und die Ladungssammlungseffizienz (CCE).

Die verwendeten Bestrahlungsanlagen sind überaus unterschiedlich was die spektrale Verteilung und Teilchenart anbelangt. Um den Strahlungsschaden auf die Neutronenenergie von 1 MeV zu skalieren wird die NIEL (Non-Ionizing Energy Loss) Hypothese angenommen.

Das Ziel dieser Masterarbeit, ausgeführt am Institut für Hochenergiephysik (HEPHY) der österreichischen Akademie der Wissenschaften, liegt darin das Spektrum des Triga Mark II Reaktors des Atominstitsts (ATI) zu charakterisieren und die korrekten NIEL Umrechnungsfaktoren der unterschiedlichen Strahlrohre auf 1 MeV Neutronen zu finden. Darüber hinaus muss das Temperaturprofil der Proben während der Bestrahlung untersucht werden. Diese Information ist essentiell für das Verständnis von zeitabhängigem Annealing von Strahlenschäden durch Diffusionseffekte.

Die approbierte gedruckte Originalversion dieser Diplomarbeit ist an der TU Wien Bibliothek verfügbar
The approved original version of this thesis is available in print at TU Wien Bibliothek.
TU WIEN Bibliothek Your knowledge hub

Die approbierte gedruckte Originalversion dieser Diplomarbeit ist an der TU Wien Bibliothek verfügbar
The approved original version of this thesis is available in print at TU Wien Bibliothek.

# Abstract

Due to its semiconducting properties silicon is a very attractive material for particle detectors in High Energy Physics (HEP). A small band gap allows relatively large signals and low noise without the need for cryogenic cooling. High charge carrier mobility implies high detector speed. Impinging particles not only cause the creation of electron-hole pairs, which are responsible for the signal by drift in an electric field, but also deteriorate the detector performance because of radiation damage.

Therefore, microscopic radiation effects like point and cluster defects of the single crystal and nuclear reaction of silicon atoms need to be studied by measuring macroscopic parameters like dark current increase, change of full depletion voltage and charge collection efficiency.

The irradiation facilities used for such investigations are very different with respect to spectral distribution and particle type. Therefore the NIEL (Non-Ionizing Energy Loss) hypothesis is used to scale the radiation damage to those of neutrons of 1 MeV energy.

The aim of this Master's thesis, performed at the Institute of High Energy Physics (HEPHY) of the Austrian Academy of Sciences, is to characterize the spectrum of the Triga Mark II nuclear reactor of the Atominstitut (ATI) and to find the correct correlation coefficients of the different irradiation channels to 1 MeV neutrons used for the NIEL scaling. Moreover, the temperature profile of the samples during irradiation need to be studied. This information is essential to understand the time-dependent annealing of radiation damage because of diffusion effects.

Die approbierte gedruckte Originalversion dieser Diplomarbeit ist an der TU Wien Bibliothek verfügbar
The approved original version of this thesis is available in print at TU Wien Bibliothek.
TU Bibliothek Your knowledge hub WIEN

Die approbierte gedruckte Originalversion dieser Diplomarbeit ist an der TU Wien Bibliothek verfügbar
The approved original version of this thesis is available in print at TU Wien Bibliothek.

# Contents


**1 Introduction** **9**

1.1 HL-LHC . . . 9

1.2 Radiation hardness studies on silicon detectors . . . 11

**2 Semiconducter Detector Fundamentals** **12**

2.1 Interaction of elementar particles with matter and signal formation . . . 12

2.2 Drift and Diffusion effects . . . 13

2.3 The planar process . . . 14

2.4 p–n junction . . . 14

2.5 Detector properties . . . 17

**3 Microscopic and macroscopic Si-detector parameters and radiation damage** **18**

3.1 Behavior of unirradiated sensors . . . 18

3.2 Microscopic radiation effects . . . 19

3.2.1 Surface damage . . . 19

3.2.2 Bulk damage . . . 19

3.3 Macroscopic consequences . . . 21

3.3.1 Leakage current . . . 21

3.3.2 Full depletion voltage and effective doping concentration . . . 21

3.4 Annealing . . . 22

3.5 Neutron capture - donor creation . . . 23

3.6 Displacement damage and NIEL scaling hypothesis . . . 24

**4 TRIGA Mark II Reactor** **26**

4.1 ATI Wien . . . 26

4.1.1 Spectrum . . . 26

4.1.2 Hardness factor Kappa . . . 30

4.1.3 Temperature profile . . . 31

4.2 JSI Ljubljana . . . 31

**5 Sample irradiation for probe carrier material** **33**

**6 Diode irradiation and measurement** **35**

6.1 Used half moons . . . 35

6.2 Half moon preparation . . . 36

6.3 Irradiation . . . 37

6.4 Measurements and annealing . . . 38

6.4.1 Measurement setup . . . 38

6.4.2 Leakage current and alpha evaluation . . . 38

6.4.3 Capacitance behavior . . . 41



Die approbierte gedruckte Originalversion dieser Diplomarbeit ist an der TU Wien Bibliothek verfügbar
The approved original version of this thesis is available in print at TU Wien Bibliothek.
TU Bibliothek Your knowledge hub WIEN

6.4.4 Frequency behavior . . . . . 44

**7 Summary and Outlook** **45**

7.1 Reactor fluence characterization and calculation for future irradiations . . 45

**8 Appendix** **47**

8.1 ATI Irradiation Procedure Manual . . . . . 47

8.2 Activation Calculation of PET . . . . . 47

8.3 Annealing Calculation . . . . . 50

8.3.1 Mathematica code . . . . . 50

8.3.2 Fortran code . . . . . 52

Die approbierte gedruckte Originalversion dieser Diplomarbeit ist an der TU Wien Bibliothek verfügbar
The approved original version of this thesis is available in print at TU Wien Bibliothek.
TU WIEN Bibliothek Your knowledge hub

# 1 Introduction

## 1.1 HL-LHC

The Large Hadron Collider (LHC) is the largest machine ever built by mankind. The circumference of the accelerator is 27 km. The LHC is the last and largest accelerator in a series of pre accelerators. A sketch of the accelerator complex with the main experiments is given in figure 1. The accelerator tunnel and the four main experiments ATLAS, ALICE,

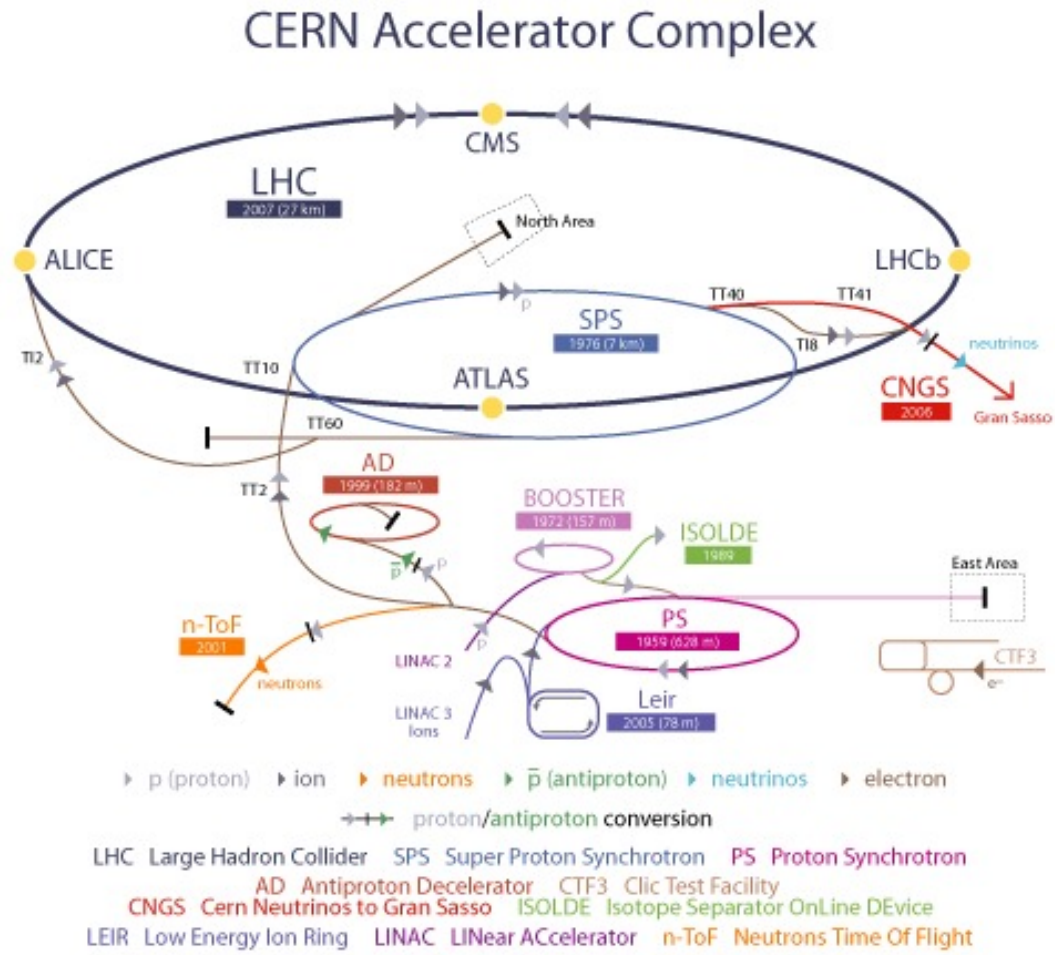


Figure 1: Sketch of the Large Hadron Collider with the four main experiments (yellow dots) and the pre accelerator complex [1]

CMS and LHC-B are located at the border area between Switzerland and France near Geneva. The design center of mass energy is 14 TeV for proton - proton collisions. The first protons entered the accelerator in 2008. The first run was performed with decreased collision energy. The plan was to collect data and then shut down for upgrades repeatedly (Long Shutdown - LS). The project schedule is displayed in fig. 2. In every shutdown major improvements to the collider and detector performance were done. Without any improvements in collision rate the scientific gain after Run 3 disappears. For further scientific research a major upgrade to the so called High Luminosity (HL) or HiLumi LHC is planned. The Luminosity $L$ is one of the parameters to describe the performance



Die approbierte gedruckte Originalversion dieser Diplomarbeit ist an der TU Wien Bibliothek verfügbar
The approved original version of this thesis is available in print at TU Wien Bibliothek.
TU Bibliothek Your knowledge hub WIEN

Figure 2: Project schedule for the LHC / HL-LHC upgrade[2]

of particle accelerators. It describes the number of collisions per area and per time with respect to the interaction cross section. Usually the unit is expressed in $b^{-1} \cdot s^{-1}$. A semiqualitative derivation of $L$ is given in [3]. With the (interaction) cross section area unit barn $b$. 1 barn is the area of $10^{-28}\,\mathrm{m}^2$. The integrated luminosity is the time integral of the luminosity and describes the total number of occurred collisions in the considered period of time.

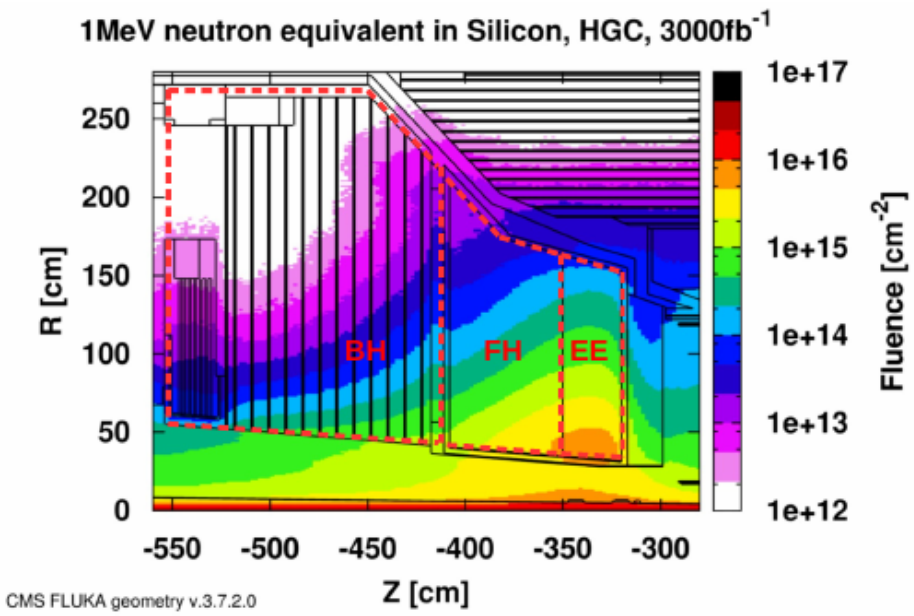


Figure 3: FLUKA[1] simmulation of the expected particle fluence in the HL-LHC CMS forward endcap calorimeter (HGC)[4]

Die approbierte gedruckte Originalversion dieser Diplomarbeit ist an der TU Wien Bibliothek verfügbar
The approved original version of this thesis is available in print at TU Wien Bibliothek.
TU Bibliothek Your knowledge hub WIEN

With the HiLumi upgrade, the instantaneous luminosity of the machine will improve by a factor of 5 and the integrated luminosity will increase by a factor of 10 compared to the original design values [5]. After the upgrade the HL-LHC will produce an integrated luminosity of ~3000 $\mathrm{fb}^{-1}$. This will exceed the design limits of the current semiconductor detectors. With the increased luminosity, not only new detectors are required, but also improvements in the radiation hardness of the future detectors. The expected fluence in the HL-LHC CMS forward endcap detector is given in fig. 3. Future experiments with even higher particle energies, fluences and luminosities require even better detector improvements.

## 1.2 Radiation hardness studies on silicon detectors

Detector studies are performed at various test sites and can be done with different types of particles [6]. The particle type determines whether bulk or surface damages occur. Reactor neutrons and high energy protons are used to study bulk defects, X-rays for surface damages. X-rays are easy to produce and don't require special facilities. For proton irradiations, the Karlsruhe Institute of Technology (KIT) run a well established proton cyclotron irradiation facility[2]. At the microscopic level, radiation damage has many effects. Detector degeneration occurs due to the creation of additional recombination centers and depletion of minority charge carriers. Mitigation for radiation hardening is achieved by selection of special dopant isotopes and substrate with wide band gap. Miniaturization also makes an important contribution to radiation hardness. The more or less stationary holes in thin structures have the ability to tunnel out of the oxide layer and vanish for the threshold energy. The effects of radiation on silicon detectors will be studied in chapter 3.

However, this thesis treats irradiations with reactor neutrons. Such tests are usually performed at the Jožef Stefan Institute[3] (JSI) TRIGA Mark II reactor in Ljubljana and the Rhode Island Nuclear Science Center[4] (RINSC) research reactor at Brown University. These JSI reactor is well understood in terms of spectrum, temperature profile and fluence. The RINSC reactor is newly commissioned for sensor irradiations but the reactor properies are not yet well comprehended. Therefore the RINSC has the unique capability to irradiate 8" wafers. Unfortunately, the transport with cooling and temperature monitoring is complex and the irradiation is expensive.

Computer simulations appear to be an inexpensive alternative. The problem with simulations is that there is no underlying theoretical model. All calculations are based on parameterized real measurements.

The aim of this master thesis is to characterize and understand the TRIGA Mark II reactor at the Atominstitut for future HEPHY[5] irradiation studies.

[2] https://www.etp.kit.edu/english/264.php
[3] https://www.ijs.si/ijsw/JSI
[4] http://www.rinsc.ri.gov
[5] https://www.oeaw.ac.at/hephy/



Die approbierte gedruckte Originalversion dieser Diplomarbeit ist an der TU Wien Bibliothek verfügbar
The approved original version of this thesis is available in print at TU Wien Bibliothek.
TU Bibliothek Your knowledge hub WIEN

# 2 Semiconducter Detector Fundamentals

Silicon is the most used material for semiconductor detectors in High Energy Physics. The small band gap enables relatively large signals and low noise without the need for cryogenic cooling. The specific resistance of semiconductors is between $10^{-3}$ and $10^{8}\,Ohm*cm$. The metalloid Si is made from $SiO_2$ quartz sand. The Oxygen is reduced with pure Carbon in arc furnaces. Detector grade silicon has impurities less than $1\times10^{-9}\,\mathrm{cm}^{-3}$. The two ways to grow silicon monocrystals are the Czochralski method and the float zone method. A detailed description is treated in [7] chapter 2.1, [8] chapter 10 and [9] chapter 3. This chapter is the theoretical silicon semiconductor background. At the beginning a brief overview about particle - detector interaction and the underlying principles is given. Then wafer production, p-n interaction and properties are discussed.

## 2.1 Interaction of elementar particles with matter and signal formation

Particles have to interact somehow with matter to be detected. With every interaction the incident particle deposits energy in the material. Particles can interact in several different ways:

- Ionization and excitation
- Bremsstrahlung
- Photon absorption and photon scattering
- Cherenkov radiation
- Nucleus interaction
- Weak nuclear force

Incoming particles usually interact with matter in different ways. The interaction is described by the scattering cross section $\sigma$. The cross section is a material dependent property and describes the probability of interaction. The interaction is dependent from the type of particle and its energy. The measurand is an effective interaction area and its unit is Barn (1 barn = 1 b = $10^{-24}\,cm^2$). A detailed description about interaction and scattering cross section is given in [10]. The mean energy loss per length unit is described by the Bethe-Bloch-equation:

$$-\left\langle\frac{dE}{dx}\right\rangle = n\int_{T_{min}}^{T_{max}} T\frac{d\sigma_A}{dT}(M,\beta,T)dT \tag{1}$$

n is the density and A further properties of the target material. $\frac{d\sigma_A}{dT}$ describes the differential interaction cross section for the energy loss by the kinetic energy T. $\beta$ and M are



Die approbierte gedruckte Originalversion dieser Diplomarbeit ist an der TU Wien Bibliothek verfügbar
The approved original version of this thesis is available in print at TU Wien Bibliothek.
TU Bibliothek Your knowledge hub WIEN

the velocity and mass of the incident particle. The equation is applicable up to energies where radiation loss effects begin to occur.

The major advantage of semiconductor detectors is the low ionization threshold energy. This means an incident particle with given energy loss per interaction produces more electron-hole pairs than in gaseous detectors. In silicon detectors the most relevant interaction is ionization. From the crystal structure and energy band regime Si is extremely interesting. Valence and conducting band are separated by a small band gap. The silicon band gap is 1.12 eV. This means the energy distance can be overcome by thermic vibration or external electric fields.When a bond is broken, an electron-hole pair is created that corresponds to free charge carriers in the conduction and valence bands. An electric field leads to moving charge carriers and thus to a current. The energetic band structure depends on temperature and pressure. Pressure reduces the atomic distance in the lattice and leads to a smaller band Gap. Raising temperature also reduces the band gap. The energy-momentum dispersion relationship must be examined for a detailed description of the band structure. (See [11] chapter 8.2.3.) We assume a particle passed through the detector and created e / h pairs in the active detector volume. Voltage is applied. The electrons and holes are now accelerated in the electric field to the electrodes (front and rear levels of the structure) and the moving charges induce a charge on the electrode surface. The electric induction is measured as a current or voltage signal and can be used directly for further data processing. The signal is generated when the charges move relative to the electrodes and not necessarily when they reach them (Ramo theorem). So charge collection at the electrodes is not the main cause for signal generation. The faster the charges move, the higher the signal gets. If the electrons and holes stop moving (trapping) or arrive at the electrodes the signal vanishes.

## 2.2 Drift and Diffusion effects

The Boltzmann transport equation describes the charge carrier movement in semiconductors. In particular the diffusions and drift movement of electrons and holes. In the most general way the Boltzmann equation is the total time derivative of a density function $f(\vec{r}, \vec{v}, t)$ and consists of three terms. The external (electrical) force term, the diffusion term and in addition a collision term (internal).

$$\frac{df}{dt} = \left(\frac{\partial f}{\partial t}\right)_{\text{force}} + \left(\frac{\partial f}{\partial t}\right)_{\text{diff}} + \left(\frac{\partial f}{\partial t}\right)_{\text{coll}} \tag{2}$$

With Hamilton's equation Boltzmann showed

$$\frac{df}{dt} = \left(\frac{\partial f}{\partial t}\right)_{\text{coll}} . \tag{3}$$

After expressing the total differential in location and velocity notation, the transport and field term rewrite to $\frac{d\vec{r}}{dt}\vec{\nabla}_{\vec{r}} f$ and $\frac{d\vec{v}}{dt}\vec{\nabla}_{\vec{v}} f$. The transport term describes the movement in



Die approbierte gedruckte Originalversion dieser Diplomarbeit ist an der TU Wien Bibliothek verfügbar
The approved original version of this thesis is available in print at TU Wien Bibliothek.
TU Bibliothek Your knowledge hub WIEN

position space, which is the macroscopic expression of diffusion. Rewriting 2 yields to

$$\frac{df}{dt} = \frac{\partial f}{\partial t} + \frac{d\vec{r}}{dt}\vec{\nabla}_{\vec{r}} f + \frac{d\vec{v}}{dt}\vec{\nabla}_{\vec{v}} f = \frac{\partial f}{\partial t}_{|coll}. \tag{4}$$

On the microscopic level the Boltzmann transport equation 4 describes the distribution in phase space. On the macroscopic level the solutions describe diffusion and drift.

An important statement of the transport equation is that time-independent electric fields induce a stationary drift movement of the charge carriers. In addition to the vectored movement in the field, an undirected thermal movement causes a drift movement of electrons and holes in areas of different concentration. For more information see [11], chapter 4.

## 2.3 The planar process

The planar process is the procedure of making semiconductor detectors or in general microchips out of Si wafers. The monocrystalline Si ingots are 12" in diameter. Before detector production can start, the ingots are cut into thin wafers of two hundred to three hundred micrometer. Back in the fifties of the last century the planar process was a ground shaking new production method using the masking and passivating properties of silicon dioxide. The first step of all is to oxidize the wafer above 1000 °C and cover it with an even $SiO_2$ layer. Then the oxide layer is covered with a photoresist (on one side) and selectively exposed to light by photomasks. This allows to selectively etch the oxide layer for further manipulation. After cleaning the structure it is implanted with doping atoms by ion bombardment. Now the structure is heated to several hundred degrees in order to evaporate the doping atoms on the oxide layer and to heal lattice defects. The process of layer deposition (can also be metal vapor deposition) and selective removal is repeated until the structure is complete. A sketch of the process is given in fig. 4

## 2.4 p–n junction

Usually silicon is doped with impurity atoms to expand the field of application. There is p (positive) and n (negative) doping. Positive means there are more holes and n means more electrons. In this context, it is important to understand the difference between minority and majority charge carriers. In p-doped material, minority charge carriers are electrons and in n-doped material holes take over this task. For majority charge carriers its vice versa. The naming of minority and majority is simply due to the greater amount of majority than minority carriers.

The Boltzmann transport equation (equation 4) is describing the charge carrier movement in semiconductors. Less or higher doping is denoted by a superscript $^-$ or $^+$ (e.g.

[6] Taken from https://www.physik.fu-berlin.de/en/einrichtungen/ag/ag-franke/courses/Abstracts-SoSe13/Talk-Hansen.pdf, Slide 27



Die approbierte gedruckte Originalversion dieser Diplomarbeit ist an der TU Wien Bibliothek verfügbar
The approved original version of this thesis is available in print at TU Wien Bibliothek.
TU Bibliothek Your knowledge hub WIEN

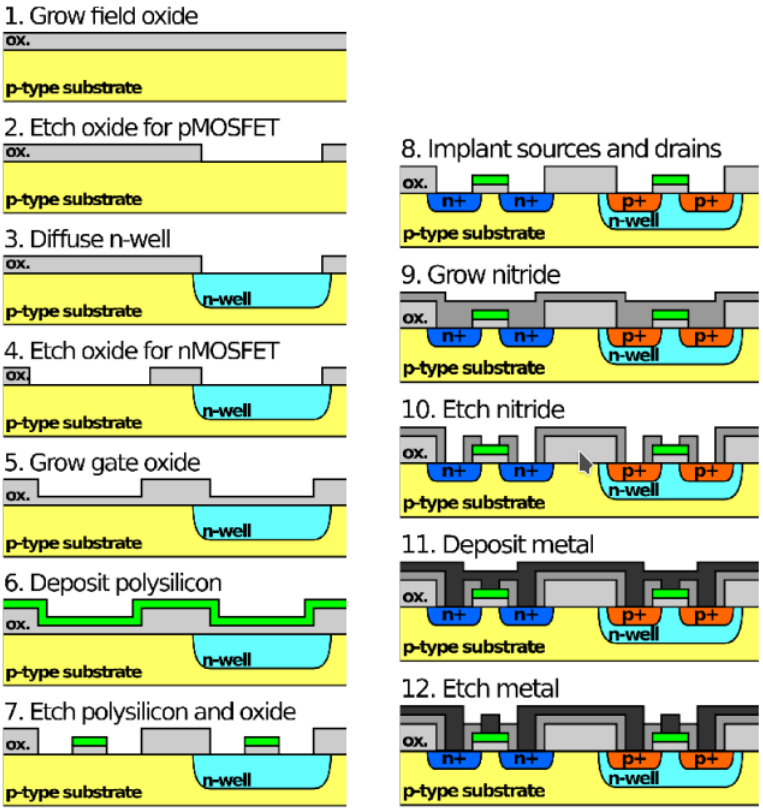


Figure 4: Planar process drawing of a simple MOSFET[6]
First the naked wafer (substrate) is covered with an oxide layer. Then layer deposition and selective removal are repeated until the structure is complete.

$n^-$ or $p^+$). Doped semiconductors are called extrinsic semiconductors. The doping is realized by ion implantation, diffusion of doping atoms or epitaxial growth.

If n and p doped layers are brought together, a so called p-n-junction is formed. This arrangement is also called Diode. The strong charge carrier difference at the p-n boundary leads to a diffusion current $I_{diff}$. By recombination of electrons and holes a depleted zone is built. The depletion zone is is also called space charge region, space charge region or junction region. The zone is dominated by the ion lattice structure and due to that not electrically neutral. There an intrinsic electric field leads to a drift current $I_{drift}$ with the opposite direction to the diffusion current. The behavior of the forward and reverse biased p-n junction is illustrated in fig. 5.

In the state of equilibrium, this zone is electrically neutral to the outside. The space charge range (SCR) is also only dependent on the doping concentration. Due to the electrical properties, the depletion zone mainly yields into the lower doped material. The width of the SCR is given in the next section in formula 6.

The conductivity of the junction depends on the externally applied voltage. Forward bias ($U_{ext} > 0$) means applying the positive voltage to p-side. This reduces the width of the depletion region and lowers the drift current in comparison to the diffusion current. A narrow depletion region means a significant forward current. Reverse bias ($U_{ext} < 0$)



Die approbierte gedruckte Originalversion dieser Diplomarbeit ist an der TU Wien Bibliothek verfügbar
The approved original version of this thesis is available in print at TU Wien Bibliothek.
TU Bibliothek Your knowledge hub WIEN

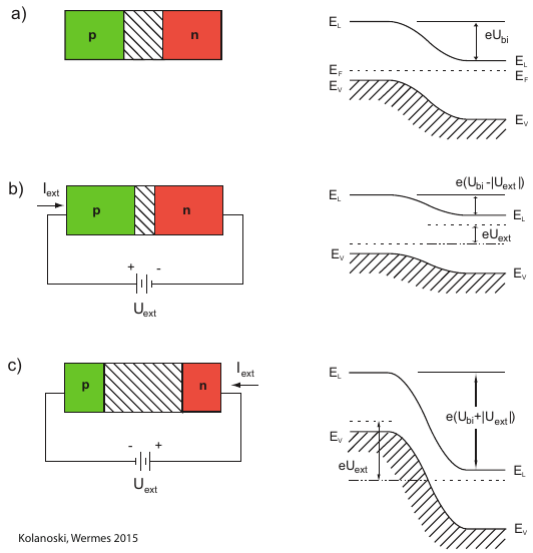


Figure 5: Behavior of the forward and reverse biased pn junction. a) no external voltage, b) external voltage in forward direction, c) external voltage reverse direction. Taken from [11], fig. 8.18. Note the different width of the depletion zone.

expands the depletion area and the diffusion current becomes smaller. This yields to a small reverse current. The forward and reverse biased behavior is illustrated in fig. 6. Apart from the detector application, this behavior is used for AC/DC current modulation. Since it is not necessary to determine the exact parameters in this work, see [11] and [7] for a deeper understanding.

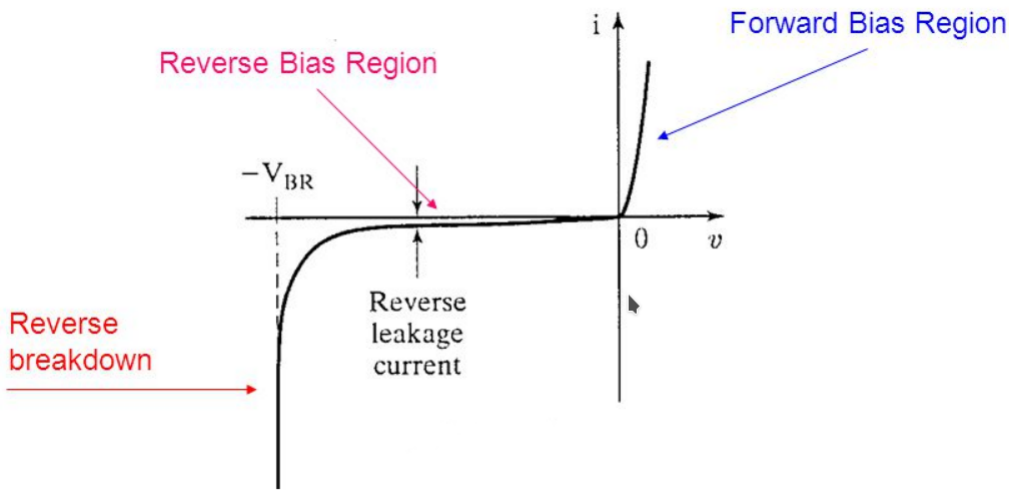


Figure 6: Current and voltage behavior of a forward and reverse biased diode[7]

Charge carriers normally diffuse at p - n junctions and especially after radiation induced defects in the semiconductor material.

[7] https://slideplayer.com/slide/5186283/16/images/2/Graphical+PN-Junction+Diode+V-I+Characteristic.jpg



Die approbierte gedruckte Originalversion dieser Diplomarbeit ist an der TU Wien Bibliothek verfügbar
The approved original version of this thesis is available in print at TU Wien Bibliothek.
TU Bibliothek Your knowledge hub WIEN

## 2.5 Detector properties

The properties discussed in the following are the current-voltage (IV) behavior, in special the leakage current and the capacitance of diodes. The current behaves in an exponential manner dependent on the external applied voltage. The Shockley equation

$$I = I_S(e^{\frac{eU_{ext}}{kT}} - 1) \tag{5}$$

is the describing model. $I_S$ is the reverse bias saturation current. This current is a material, area and doping dependent constant of the (ideal) diode. Semiconductor particle detectors are usually reverse biased to full depletion. The depleted zone is the active volume for particle detection. The deposited energy in the depleted zone creates electron - hole pairs and leads to a detectable current. The active thickness d can be calculated over the external applied voltage.

$$d \approx \sqrt{\frac{2\epsilon\epsilon_0}{e}\frac{1}{N_D}(U_{bi} + U_{ext})} \approx 3.6 \cdot 10^3 \sqrt{\frac{U_{ext}}{N_D(\mathrm{Vcm})}} \tag{6}$$

The depletion zone of a diode can be considered as a dielectric in a plate capacitor. The capacitance C of a simple plate capacitor is:

$$C = \frac{\epsilon \cdot \epsilon_0}{d} \cdot A \tag{7}$$

A is the area and d the width of the depletion zone of the diode. Since the width of the diode has a built in value the capacitance trends to a constant. In the later chapter 6.3 the capacitance is measured and the data is used to determine the $V_{fd}$. For reverse biased diodes a strong temperature-dependent ($\propto T^2$) leakage current is observed. The leakage current has volume and surface parts. The volume part is $\propto \sqrt{U_{ext}}$ due to width dependency and the surface part is $\propto U_{ext}$. Leakage current measurement is an important method for determining radiation damage and is typically of the order of $nA/cm^2$, but becomes $\mu A/cm^2$ after strong irradiation.

Die approbierte gedruckte Originalversion dieser Diplomarbeit ist an der TU Wien Bibliothek verfügbar
The approved original version of this thesis is available in print at TU Wien Bibliothek.
TU WIEN Bibliothek Your knowledge hub

# 3 Microscopic and macroscopic Si-detector parameters and radiation damage

Leakage current, full depletion Voltage $V_{fd}$ and Charge Collection Efficiency CCE are the most relevant macroscopic detector parameters. The leakage current is derived form reverse biased IV measurements and the full depletion voltage from CV data. CCE for silicon is almost 100 % for fluences up to $10^{15}$ cm$^{-2}$. In the case of higher irradiated sensors, trapping[12] (of charge carriers) leads to a decrease in the CCE. Most of the behavior of irradiated sensors can be reduced to the treatment of doping effects. Amongst others, doping is affected by neutron capture (see 3.5). Fig. 7 shows the schematic principle of space charge, trapping and leakage current.

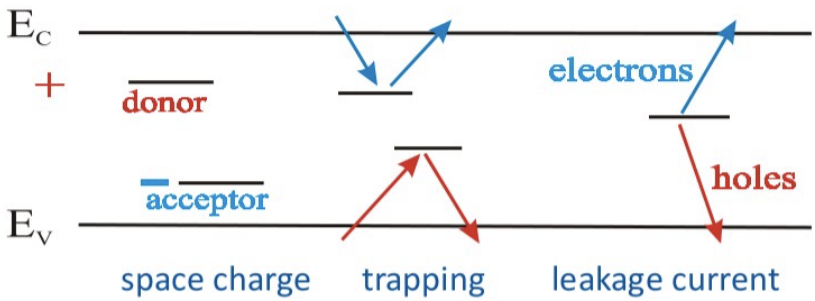


Figure 7: Schematic principle of space charge, trapping and leakage current with the conduction $E_C$ and valence $E_V$ bands.[13]

Diffusion and drift are important for the detector understanding during operation and under maintenance. Diffusion is also important to treat annealing of radiation defects. Radiation creates point and cluster damage at the grid level. For more information see introductory works in materials science and [7] (chapter 3.3 and 6).

## 3.1 Behavior of unirradiated sensors

Due to the usage of the full detector volume, the area of operation of a particle detector is beyond the full depletion voltage but below breakdown voltage. The full depletion voltage is determined from CV measurements. A typical CV curve of an unirradiated diode is given in fig. 8. The green line indicates the $V_{fd}$ of the structure. The dark current before the breakthrough is a quality criterion for the impurity density. Impurities add additional energy levels in the band gap and thereby significantly influence the detector behavior. A typical IV curve is given in fig. 9.



Die approbierte gedruckte Originalversion dieser Diplomarbeit ist an der TU Wien Bibliothek verfügbar
The approved original version of this thesis is available in print at TU Wien Bibliothek.
TU Bibliothek Your knowledge hub WIEN

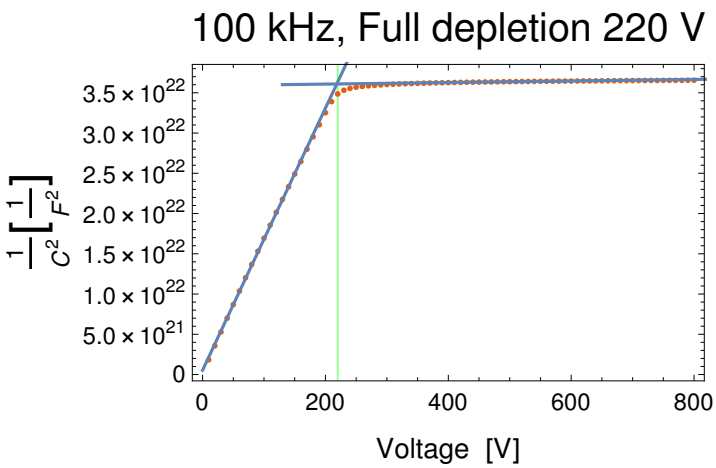


Figure 8: Typical CV curve of an unirradiated diode with linear fits to determine the $V_{fd}$

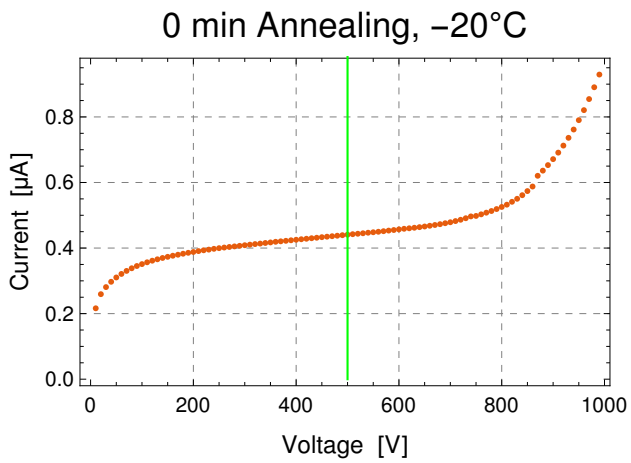


Figure 9: Typical IV curve of a cooled structure. The green line indicates the corresponding full depletion voltage.

## 3.2 Microscopic radiation effects

### 3.2.1 Surface damage

Radiation causes ionization and displacement damage in the $Si - SiO_2$ boundary layer. Due to the applied voltage and the high fields in sensors, immediate recombination is inhibited. The mobility of holes in $SiO_2$ is $10^6$ times lower than of electrons. Holes are trapped in the $Si - SiO_2$ boundary layer in deep energy levels and contribute to the stationary oxide charge. The influence of the detector operation is negligible for surface damage. In contrast, the influence on integrated circuits is considerable.

### 3.2.2 Bulk damage

The damage of the bulk material of the detector is mostly caused by non-ionizing effects. This damage has far-reaching effects on the operation and performance of the detector. Especially the charge collection efficiency is highly effected in irradiated semiconductor



Die approbierte gedruckte Originalversion dieser Diplomarbeit ist an der TU Wien Bibliothek verfügbar
The approved original version of this thesis is available in print at TU Wien Bibliothek.
TU Bibliothek Your knowledge hub WIEN

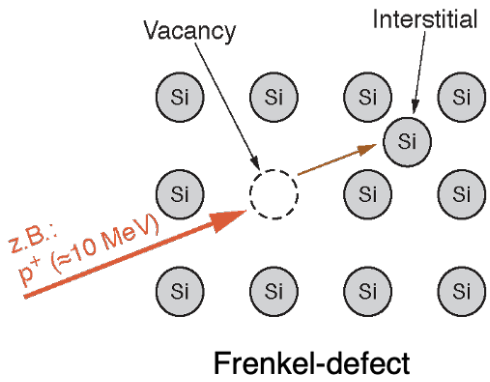


Figure 10: Frenkel defect with the interstitial atom on the right corner[13]

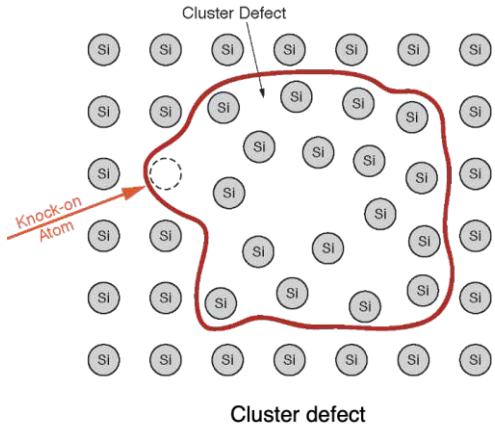


Figure 11: Widespread dislocation - cluster defect[13]

sensors.

Apart from boundary layers, ionization is a reversible process in semiconductor materials. Due to non-ionizing events, cores of the lattice can be thrown out of their lattice position or occupy interstitial spaces (Frenkel-defect). Lattice damages are movable in the bulk material and can form stable damagebindings. In addition the knocked out atom can hit further nuclei. This mechanism causes cluster damages with expansions of 10 nm x 200 nm[11]. Fig. 10 und 11 show Frenkel and Cluster defects. The scattering cross-section for charged particles (electrons, protons, pions, . . . ) is larger than that for neutrons. As a result, charged particles cause more point defects than neutrons. Fig. 12 displays the lattice damage for neutrons and protons with different energies.

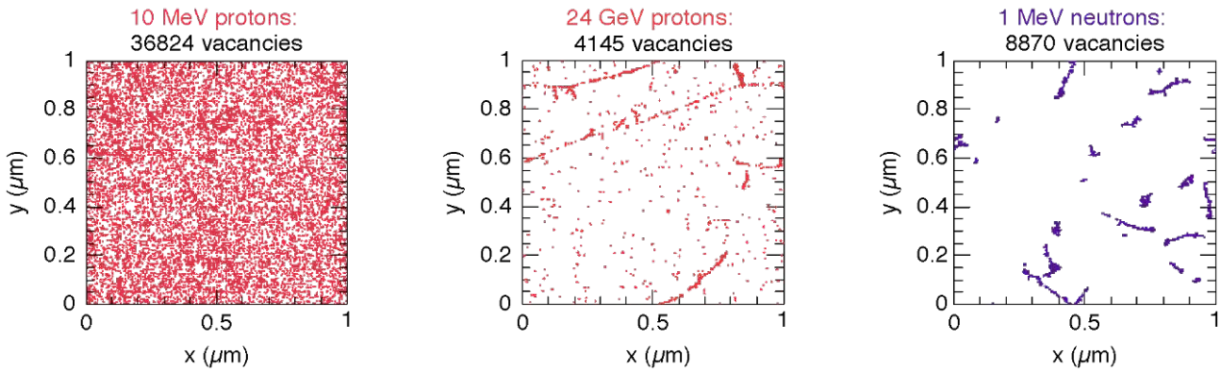


Figure 12: Lattice damage for 10 MeV and 24 GeV protons and 1 MeV neutrons of a 1 $\mu m^3$ silicon crystal volume.[13]

Die approbierte gedruckte Originalversion dieser Diplomarbeit ist an der TU Wien Bibliothek verfügbar
The approved original version of this thesis is available in print at TU Wien Bibliothek.
TU Bibliothek Your knowledge hub WIEN

## 3.3 Macroscopic consequences

### 3.3.1 Leakage current

Leakage occurs in reverse biased semiconductors and is the voltage-dependent current across the non-conductive volume. The leakage current is often reported as a leakage current density in $[\frac{A}{cm^2}]$, which is the current divided by the electrode area at a given applied voltage. However in this thesis all the diodes have the same area and the IV characteristic is evaluated in [µA].

The following formula is used to study the interplay between leakage current, voltage and the monoenergetic equivalent fluence (chapter 3.6):

$$\Delta I = \Phi_{eq} \cdot \alpha(T, t) \cdot V \tag{8}$$

$\alpha$ is called the current related damage rate .

Leakage is a strongly temperature dependent effect. With Equation 9 the measured current $I_1$ at temperature $T_1$ can be denoted to the current $I_2$ at temperature $T_2$.

$$\frac{I(T_2)}{I(T_1)} = \left(\frac{T_2}{T_1}\right)^2 \cdot e^{-\frac{E_{eff}}{2k_B} \cdot \left(\frac{1}{T_2} - \frac{1}{T_1}\right)} \tag{9}$$

The derivation of Equation 9 is given in [14] chapter 8.1.4. As rule of thumb the current doubles if the temperature increases 7 °C. In analyzing the alpha parameter the temperature dependent current has to be considered carefully. In irradiated diodes additional deep level defects produce many generation-recombination spots that affect the observable behavior.

### 3.3.2 Full depletion voltage and effective doping concentration

The full depletion voltage $V_{fd}$ is a describing parameter for operating particle detectors. To use all the available volume for particle detection one always wants to operate a detector at least nearby. There are two accepted ways to graphically determine the $V_{fd}$. The first is to fit two straight lines into the increasing and constant CV - curve parts (fig. 8). The intersection of the two straight lines indicates the $V_{fd}$. The second method is to identify the point with the strongest curvature in the CV - graph.

The first method fits well for unirradiated diodes. Irradiated diodes show a non linear increase of the $\frac{1}{C^2}$ characteristic up to the plateau, if they even have any. So the second method is better feasible. The max curvature can be calculated by the first derivative of the curvature function $\kappa$

$$\kappa = \frac{|y''|}{(1 + y'^2)^{\frac{3}{2}}}, \tag{10}$$

or simply by evaluating the minimum of the second derivative of the CV curve fit. The last method was chosen for this thesis (chapter 6). According to [14] chapter 8.3.1 the



Die approbierte gedruckte Originalversion dieser Diplomarbeit ist an der TU Wien Bibliothek verfügbar
The approved original version of this thesis is available in print at TU Wien Bibliothek.
TU Bibliothek Your knowledge hub WIEN

error of the $V_{fd}$ is up to ± 20 V in the evaluation.

The effective doping concentration $N_{eff}$ of the bulk material can be determined via the $V_{fd}$ of the sensor with

$$\mathrm{V_{dep}} \approx \frac{\mathrm{e_0}}{2\varepsilon\varepsilon_0}|\mathrm{N_{eff}}|\mathrm{d}^2. \tag{11}$$

$e_0$ is the elementary charge and d the active thickness of the semiconductor detector.

## 3.4 Annealing

Radiation induced defects have huge impact on detector functionality. Radiation creates defects and dislocations in the crystal lattice. Moreover the effective doping concentration $N_{eff}$ changes due to donor removal and acceptor generation. The Hamburg model [15] is the description of the radiation induced change of the $N_{eff}$ before and after irradiation. Thermal heating is used to heal radiation damage. This process is called annealing. $N_{eff}(\Phi_{eq}, T, t)$ is assigned with annealing time t at temperature T. The Hamburg model is a simplified annealing function consisting of three terms:

$$\Delta N_{eff}(\Phi_{eq}, T, t) = N_A(\Phi_{eq}, T, t) + N_C(\Phi_{eq}) + N_Y(\Phi_{eq}, T, t) \tag{12}$$

With $N_A$ the short-term oder beneficial annealing, $N_C$ the stable damage and $N_Y$ the reverse annealing. The beneficial annealing can be expressed as a sum of exponentials:

$$N_A(\Phi_{eq}, T, t) = \Phi_{eq} \sum_i g_{a,i} \mathrm{e}^{-\frac{t}{\tau_{a,i}(T)}} \tag{13}$$

$N_A$ describes the temperature dependent healing of lattice damage. The stable damage has only fluence and no temperature or time dependency:

$$N_C(\Phi_{eq}) = N_{C0}(1 - \mathrm{e}^{-c\Phi_{eq}}) + g_C\Phi_{eq} \tag{14}$$

This term describes the donor and acceptor behavior. The last term represents the reverse annealing behavior:

$$N_Y(\Phi_{eq}, T, t) = g_Y\Phi_{eq}\left(1 - \frac{1}{1 + t/\tau_Y}\right) \tag{15}$$

Reverse annealing describes the effect that the voltage required for full detector depletion has to be raised over time. The fluence independent constant $\tau_Y$ is a strong hint for a first order microscopic defect reaction process. Despite that there are some other effects that are better described by second order diffusion. A detailed explanation of the three terms is given in [16]. Fig. 13 shows the annealing behavior described by the Hamburg model. The standard annealing procedure is 80 min @ 60 °C.

Annealing cannot be described solely by first or second order diffusion. Some phe-

[8] Investigation on the improved radiation hardness of silicon detectors with high oxygen concentration - fig. 1



Die approbierte gedruckte Originalversion dieser Diplomarbeit ist an der TU Wien Bibliothek verfügbar
The approved original version of this thesis is available in print at TU Wien Bibliothek.
TU Bibliothek Your knowledge hub WIEN

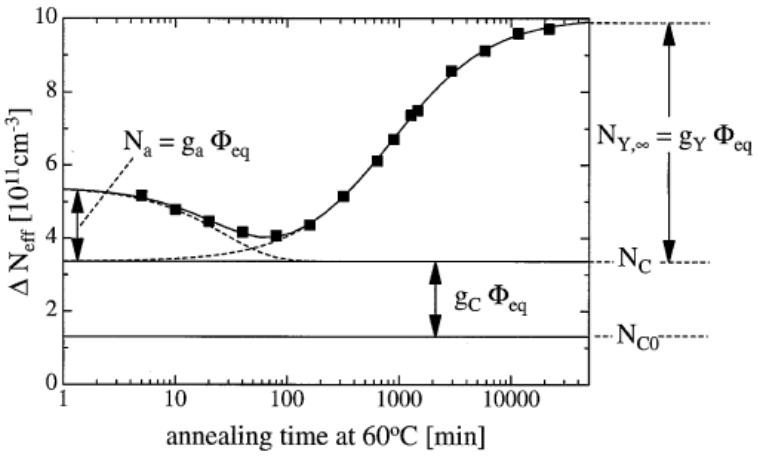


Figure 13: Simplified annealing behavior [8]

nomena can be better described by $1^{st}$ order processes and some by $2^{nd}$ order processes. One approach that has not yet been fully developed is diffusion with retention, a third-order process. This path could possibly be a closed description of the observed annealing behavior.

## 3.5 Neutron capture - donor creation

In every particle detector application and especially during reactor irradiation neutron capture occurs. In neutron capture processes, the detector substrate - in this case silicon - is usually of importance. Si has three stable isotopes: $^{28}Si$, $^{29}Si$ and $^{30}Si$. The natural occurrence of $^{28}Si$ is round 92 %. If $^{31}Si$ is produced, it naturally executes beta minus decay ($\beta^-$) to $^{31}P$.

$$^{28}\text{Si} + n \rightarrow {}^{29}\text{Si} + n \rightarrow {}^{30}\text{Si} + n \rightarrow {}^{31}\text{Si} \xrightarrow[\text{half life time}]{2.62\text{ h}} {}^{31}\text{P} + e^- + \bar{\nu}_e \tag{16}$$

This means that during detector operation, the doping concentration will change over time with the applied fluence. Hence phosphorus acts as a donor in silicon, the donor concentration rises with increasing fluence.

All other neutron capture effects can be neglected due to the low concentration of impurity atoms. Just for completeness the n and p dopants are briefly discussed. The n - doping atom phosphorus has only the single stable isotope $^{31}P$. Through neutron capture it changes to $^{32}P$ which also undergoes a $\beta^-$ decay to $^{32}S$. The p - doping atom boron exists in the stable isotopes $^{10}B$ and $^{11}B$. In radiation hardened detector applications only $^{11}B$ is used due to its greatly vanishing neutron reaction cross section.[9] [17]

Boron acts as an acceptor in silicon. So the acceptor concentration does not change in radiation hardened detectors.

[9]For more information see boron neutron cross section; 3M, isosolutions and SAID Boron-11 products.



Die approbierte gedruckte Originalversion dieser Diplomarbeit ist an der TU Wien Bibliothek verfügbar
The approved original version of this thesis is available in print at TU Wien Bibliothek.
TU Bibliothek Your knowledge hub WIEN

## 3.6 Displacement damage and NIEL scaling hypothesis

A spectrum is harder to treat than a monoenergetic case. That is why it is common in HEP and detector development to reduce a known but complex spectrum to a monoenergetic effect. The key idea behind doing so is the NIEL (Non Ionizing Energy Loss) scaling hypothesis. Five points are necessary to understand and characterize the spectrum of the Triga Mark II reactor of the ATI.

- displacement damage function [18]
- equivalent monoenergetic neutron fluence
- fluence spectrum hardness parameter
- neutron fluence and neutron fluence spectrum
- (kinetic energy released in matter - kerma)

The displacement damage function $D(E)$ (unit MeV·mbarn) is the quotient of the observable displacement damage of the target atom and the particle fluence. Each particle has its own damage function. They are difficult to determine but have been well examined in the literature. The equivalent monoenergetic neutron fluence $\phi_{eq}^{1\,\mathrm{MeV}}$ is described as the fluence of monoenergetic neutrons with a specific energy required to produce the same displacement damage in the target material as an arbitrary beam. The hardness parameter $\kappa$ is defined as the quotient of equivalent monoenergetic neutron fluence and the total fluence. The neutron fluence $\boldsymbol{\phi}$ and the neutron fluence spectrum $\phi$(E) of the source have to be known or predetermined.

In the following equation,

$$\phi_{eq}^{1\,\mathrm{MeV}} = \kappa \cdot \boldsymbol{\phi} \tag{17}$$

the hardness parameter can be calculated with

$$\kappa = \frac{\int_{E_{min}}^{E_{max}} D(E) \cdot \phi(E) dE}{95\,\mathrm{MeV} \cdot \mathrm{mbarn} \int_{E_{min}}^{E_{max}} \phi(E)}. \tag{18}$$

95 MeV · mbarn is according to [19] the displacement damage reference value designated for silicon and for the specified equivalent energy of 1 MeV. Figure 14 shows the displacement damage function for neutrons. The values have been tabulated by A. Vasilescu and G. Lindstroem after the work of [20].

In chapter 4, the NIEL hypothesis, and in particular the formula 18, is used to determine the hardness factor of the ATI TRIGA reactor. In the following the relevant (neutron) energies of Si are discussed. In silicon the minimal threshold energy for lattice displacement is 25 eV [21]. The minimum kinetic neutron energy for generating Frenkel pairs is 185 eV and 35 keV for cluster damage. As can be seen in fig. 14, the damage

[10] Data taken from `https://rd50.web.cern.ch/NIEL/neutrons.pdf`



Die approbierte gedruckte Originalversion dieser Diplomarbeit ist an der TU Wien Bibliothek verfügbar
The approved original version of this thesis is available in print at TU Wien Bibliothek.
TU Bibliothek Your knowledge hub WIEN

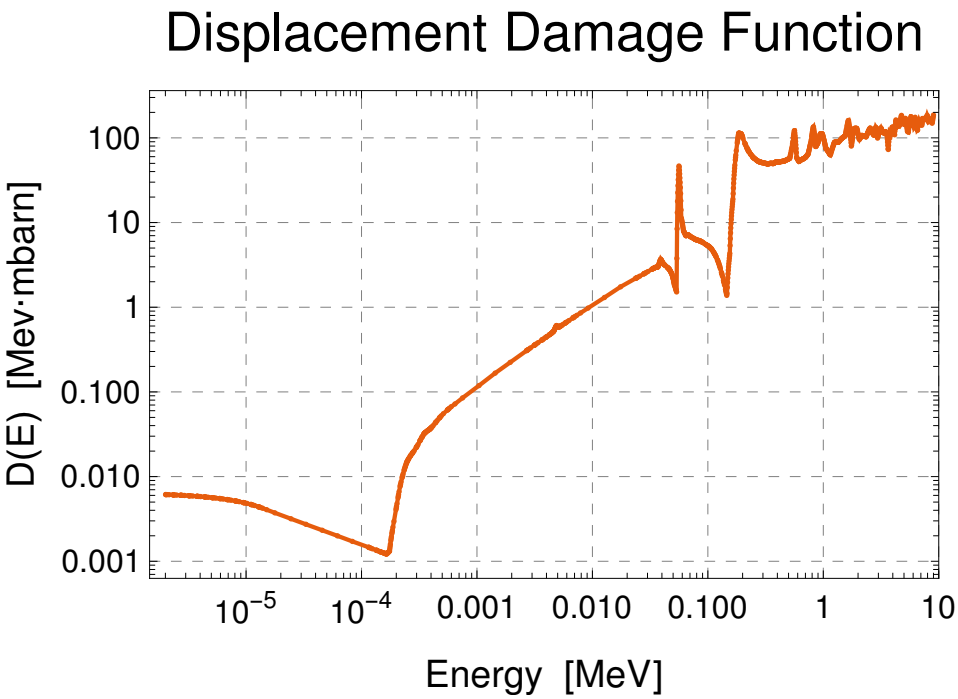


Figure 14: Neutron displacement damage function D(E) for silicon[10].

function increases with decreasing energy. The reason for this is neutron capture. During this process, the atom receives recoil energy by emission of a 1 keV photon. Since 1 keV > 25 eV, lattice damage is caused due to recoil energy.

Die approbierte gedruckte Originalversion dieser Diplomarbeit ist an der TU Wien Bibliothek verfügbar
The approved original version of this thesis is available in print at TU Wien Bibliothek.

# 4 TRIGA Mark II Reactor

The TRIGA (Training, Research, Isotope production, General Atomics) Reactor is a pool-type nuclear research reactor produced by General Atomics (GA). The power range yields from a few kW to some MW. The idea goes back to US President Eisenhower's speech "Atoms for Peace". The reactor is inherently safe - that means safe by nature and not merely by technology. Edward Teller once said ". . . a reactor so safe that it could be given to a bunch of high school children to play with without any fear that they would get hurt . . .". The prototype went critical on 3rd May 1958 at the GA test site in San Diego. From that time on more than 60 TRIGA type reactors were built all over the globe. Originally the reactor was operated with High Enriched Uranium (HEU) that contained about 70 % $^{235}U$. Since the late eighties modified fuel elements with Low Enriched Uranium (LEU) with about 19 % $^{235}U$ have to be used due to political decisions. The moderator is zirconium hydride and the water is just coolant. In addition the reactor is surrounded by a graphite neutron reflector.

## 4.1 ATI Wien

The TRIGA Mark II reactor at the Atominstitut is critical since 7th March 1962. The reactor is used for pure research purposes. The area of application spans training, research and isotope production. The maximum design power rating is 250 kW. The peculiarity of the reactor is a negative temperature coefficient. This property has the consequence that the reactivity decreases with increasing temperature. All the tecnical data is accessible in [22]. Due to this long research period the reactor behavior is understood at an adequate level. For sample irradiations a variety of beam ports are available:

- 4 beam tubes with 15.2 cm in diameter
- Central beam tube (ZBR) in the core center
- 5 reflector beam tubes called "Lazy Susan"
- a pneumatic transfer system (near the core edge)
- thermal column
- irradiation room

A cross section of the reactor with the irradiation facilities is given in figure 15 and 16. The dry radiation tubes "Lazy Susan" (LS) were chosen for the irradiations required in this work due to their neutron flux, accessibility and size.

### 4.1.1 Spectrum

An important preliminary work for sample irradiations is to fully understand the reactor spectrum. Due to nuclear fission there is a certain neutron flux described in neutrons per



Die approbierte gedruckte Originalversion dieser Diplomarbeit ist an der TU Wien Bibliothek verfügbar
The approved original version of this thesis is available in print at TU Wien Bibliothek.
TU Bibliothek Your knowledge hub WIEN

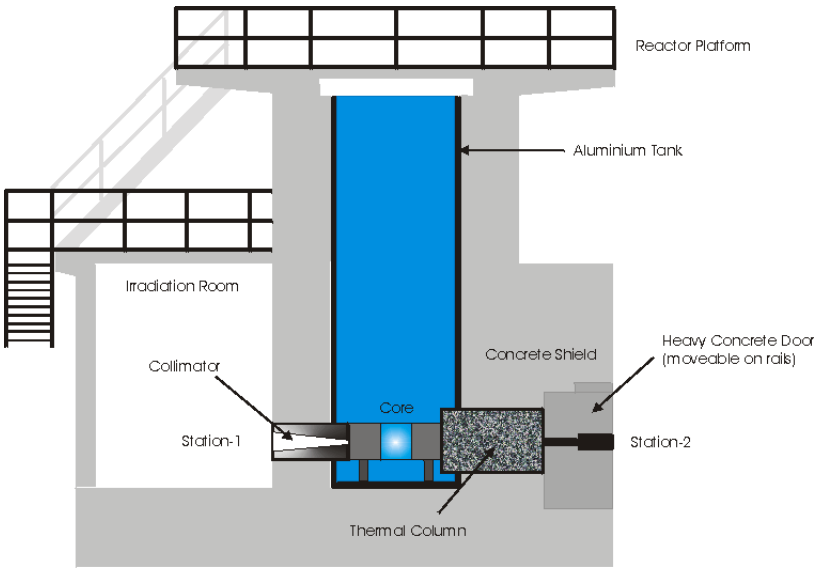


Figure 15: Vertical cross section of the ATI TRIGA Mark II reactor)

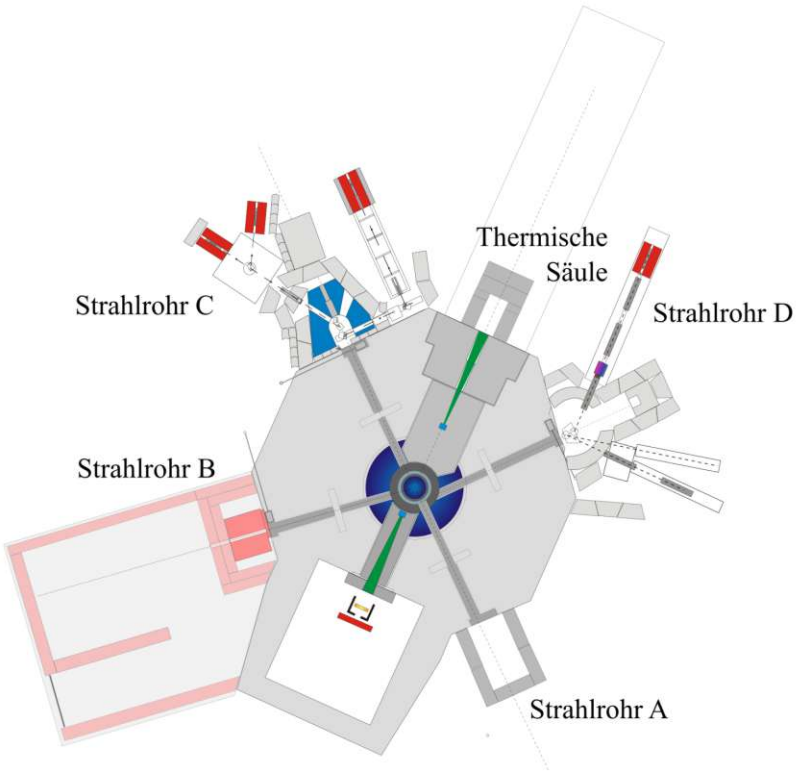


Figure 16: Horizontal cross section of the ATI TRIGA Mark II reactor

square centimeter per second. The fluence is the time integral of the flux and represents the number of neutrons per unit area. From that we derive the neutron fluence spectrum. The fluence spectrum is the energy dependent neutron fluence (partial energy derivative). In other words the fluence between $E$ and $E + \delta E$. Unfortunately, in most scientific publications, all terms are referred to only as $\phi$. So it is important to know what quantity is being treated. Two main sources are taken to specify the TRIGA reactor spectrum: The



Die approbierte gedruckte Originalversion dieser Diplomarbeit ist an der TU Wien Bibliothek verfügbar
The approved original version of this thesis is available in print at TU Wien Bibliothek.
TU Bibliothek Your knowledge hub WIEN

GA[23] table and the PhD theses of Marcella Cagnazzo[24]. The table on page 46 is the original data from GA. The data is still valid because no changes were made to the core configuration. The table consists of 24 energy fields and is visualized in figure 17. The picture on the left side is from Lazy Susan. The right one is from the central beamtube ZBR (ger: "Zentrales Bestrahlungs Rohr"). These two figures visualize the integral flux of the TRIGA reactor at the ATI Wien.

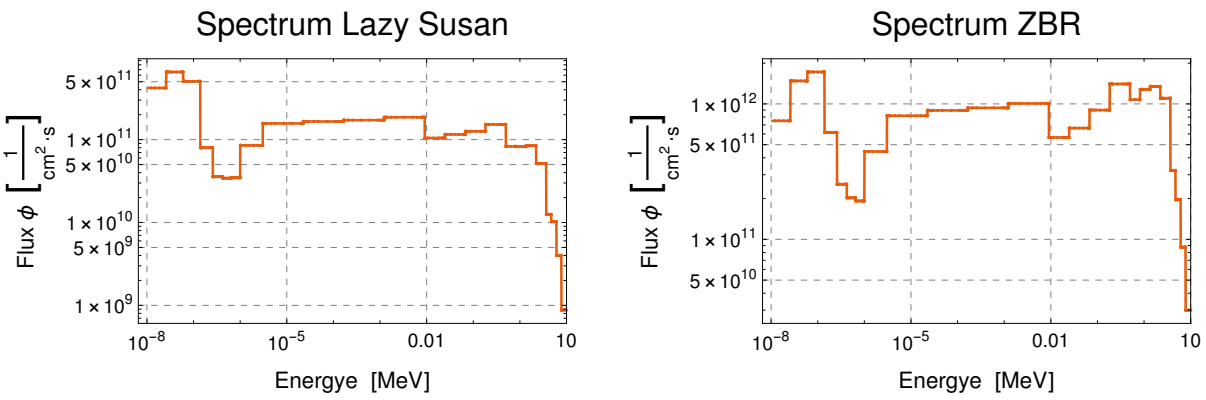


(a) LS (b) ZBR

Figure 17: Integral TRIGA step spectrum of LS and ZBR. Data taken from the original GA table

The data is compared to new foil irradiations made by Marcella Cagnazzo. In her theses she covers the differential and integral flux of the ZBR and the differential flux of Lazy Susan. Unfortunately no integral flux of LS. Her data is shown in fig. 18. As can be seen, the integral flux is qualitatively similar to the ZBR GA data in fig. 19. So the consideration is justified to say the LS fluxes also match together.

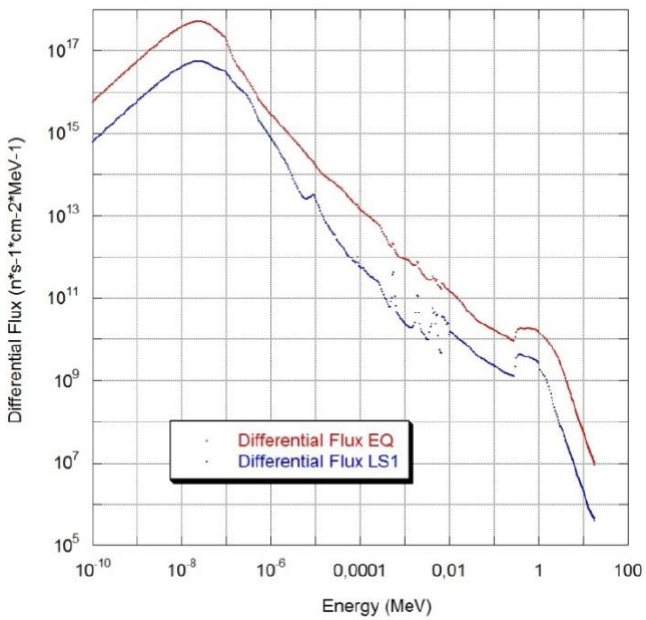


Figure 18: Plots of the spectrum from [24]: LS differential flux



Die approbierte gedruckte Originalversion dieser Diplomarbeit ist an der TU Wien Bibliothek verfügbar
The approved original version of this thesis is available in print at TU Wien Bibliothek.
TU Bibliothek Your knowledge hub WIEN

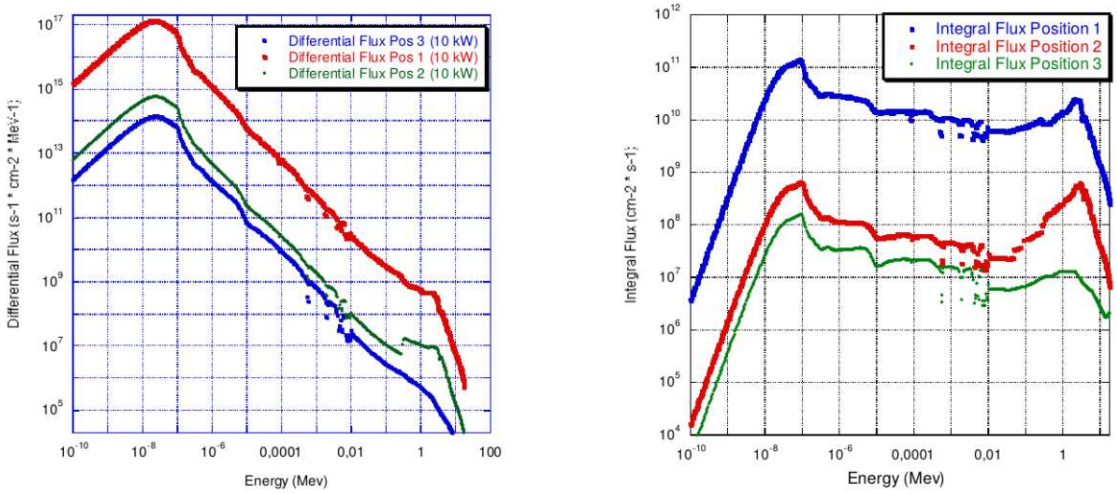


Figure 19: Plots of the spectrum from [24]: ZBR differencial and integral flux

Her spectrum is consistent with the GA data but is more accurate and contains 621 data points instead of 24. According to table 2.14 in her theses the neutron flux (in $\frac{neutrons}{cm^2 \cdot s}$) at full reactor power for LS is:

- Total flux: $3,69 \pm 0,31 \cdot 10^{12}$
- Thermal flux (<0.55 eV): $2,05 \pm 0,17 \cdot 10^{12}$
- Epithermal flux (0.55 eV - 100 keV): $5,59 \pm 0,5 \cdot 10^{11}$
- Fast flux (100 keV - 18 MeV): $1,08 \pm 0,13 \cdot 10^{12}$

For the integral (total) flux she claims 9 % uncertainty. Important to mention is, that the 5 LS tubes slightly vary in flux. The standardization is done with respect to tube 3. In figure 20 the variation of the five radiation tubes is pictured. The graphic was made by

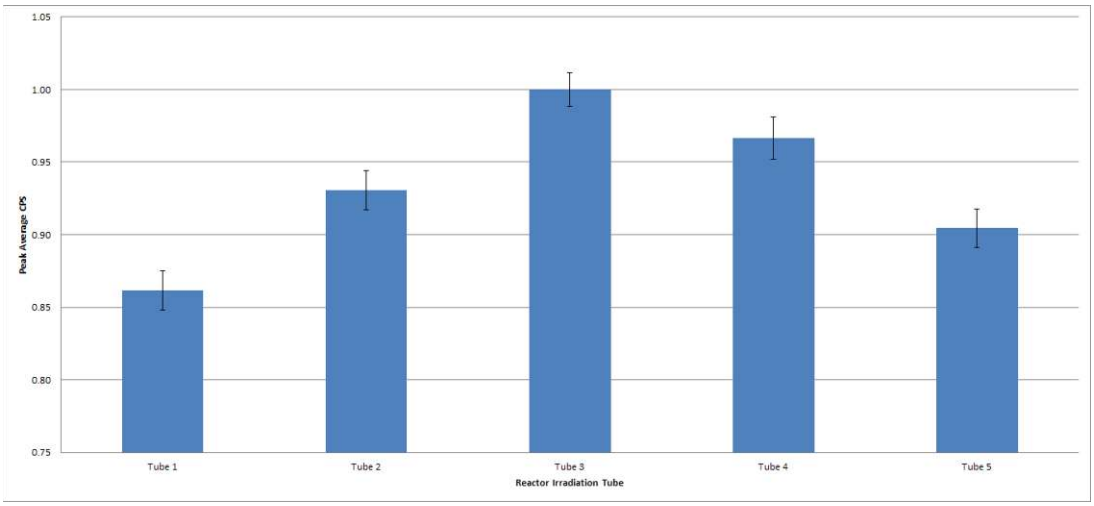


Figure 20: Flux distribution in the Lazy Susan beam tubes, normalized to tube 3 in the middle [25]

Die approbierte gedruckte Originalversion dieser Diplomarbeit ist an der TU Wien Bibliothek verfügbar
The approved original version of this thesis is available in print at TU Wien Bibliothek.

[25] in the course of Cobalt irradiations for the IAEA.

The different fluxes will be carefully attended later in section 6 when dealing with Si sample irradiations.

### 4.1.2 Hardness factor Kappa

This section is about determining the hardness factor of the Lazy Susan beam tubes of the research reactor in Vienna. In this case the reactor beam with the known spectrum $\phi$(E) and any fluence $\boldsymbol{\phi}$ is reduced to the equivalent 1 MeV neutron fluence. To calculate $\kappa$, $\phi(E)$ is multiplied with the corresponding $D(E)$ and then the integral in Equation 18 is evaluated from MIN to MAX. The product function of $D(E)$ and $\phi(E)$ is displayed in figure 21. Due

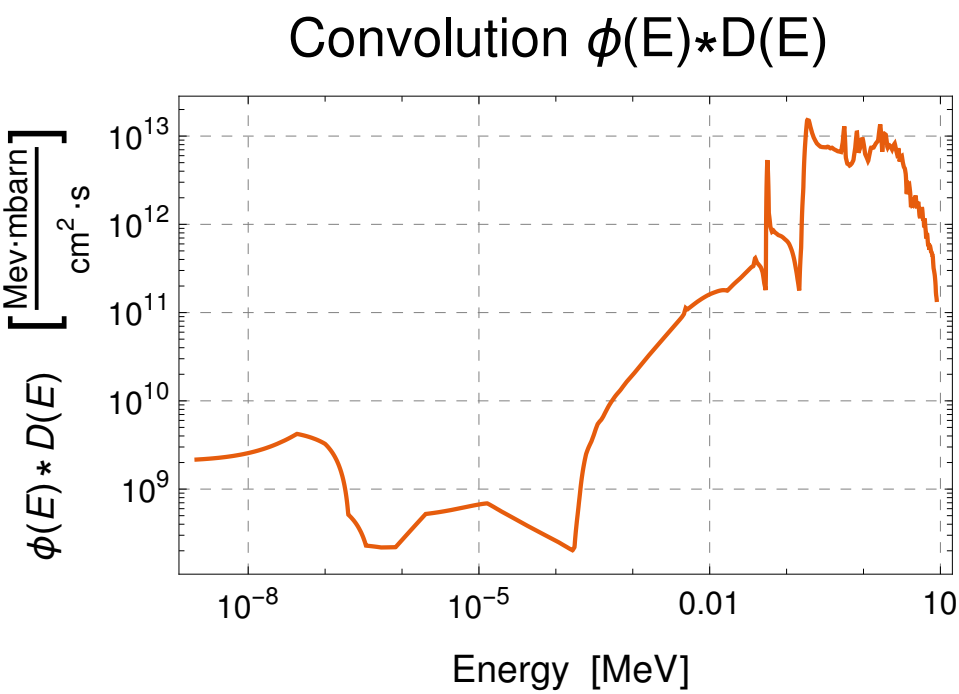


Figure 21: Plot of the product function $\phi(E)$ and $D(E)$.

to the fact that there are huge resonance effects in the displacement damage function over a wide energy field, more or less the whole energy range has to be considered. Some relevant energies for silicon have already been mentioned in chapter 3.6. In the calculation the analytical integration is not practicable since $\phi(E)$ and $D(E)$ are usually measured ore tabulated values and no analytical functions. For this work the calculation is done in Mathematica. The integration is calculated from 0.01 eV to 10 MeV. With that, kappa for the total spectrum yields to 0.138 and for energies higher than 0.1 MeV to 0.79. According to ASTM[11] A1.3 [19], a 20 % uncertainty in the spectrum does not cause more than 10 % uncertainty in the 1 MeV equivalent fluence $\phi_{eq}^{1\,\mathrm{MeV}}$. So the 13 % deviation of the LS tube 1 from the reference tube 3 thus leads to an uncertainty of the 1 MeV equivalent fluence well below 10 %.

[11] https://www.astm.org



Die approbierte gedruckte Originalversion dieser Diplomarbeit ist an der TU Wien Bibliothek verfügbar
The approved original version of this thesis is available in print at TU Wien Bibliothek.
TU Bibliothek Your knowledge hub WIEN

### 4.1.3 Temperature profile

For a useful annealing study its important to know the temperature history of the irradiated sample. Since it is undesirable to produce unnecessarily large amounts of radioactive waste, no temperature measurement was allowed during this work. The few available temperature values come from the reactor management.

- In stand by mode the reactor temperature is 22 °C.
- During operation at full power, the temperature of the cooling water in the reactor tank rises to around 40 °C. The increase of temperature takes up to 30 min.
- At full power, halfway up in the tank the temperature is ~30 °C.
- 10 minutes after switching off, the temperature is 22 °C.

No measurement was carried out in LS, so it is not clear whether the temperature in the beam tube corresponds exactly to that in the reactor tank. For further calculation this is just assumed. Based on these data an annealing estimation is performed in section 6.3.

## 4.2 JSI Ljubljana

The Jožef Stefan Institute is the long lasting expertise in irradiations. The reactor is well known in terms of fluence, dosimetry and temperature profile.

The JSI reactor runs on slightly higher $^{235}U$ than the ATI TRIGA. The higher Uranium weight percentage increases the $^{235}U$ weight from 38 g to 56 g per fuel element. This allows a 1 GW pulse instead of a 250 MW at the ATI. The JSI TRIGA has a unique triangular core modification as shown in fig. 22. The feature is that 3 fuel element places are reamed out and used as a single triangular irradiation channel. The modification allows to irradiate samples incore with diameters up to 4 cm and provides extra space for coolant or monitoring devices. More information about the modified core and all the irradiation facilities can be found in [26] and [27].

The spectrum for all the JSI irradiation tubes is displayed in fig. 23.

Fig. 24 shows a temperature measurement at full reactor power. The sensors were taken out of the reacor core after 10 min of irradiation.

In comparison to the ATI TRIGA, kappa for the total spectrum is 0.146 and for energies higher than 0.1 MeV it is 0.83. The difference is solely rooted in the modified reactor core and the slightly different fuel elements.

[12] Taken from [26] fig. 3
[13] Taken from [27] Slide 52



Die approbierte gedruckte Originalversion dieser Diplomarbeit ist an der TU Wien Bibliothek verfügbar
The approved original version of this thesis is available in print at TU Wien Bibliothek.
TU Bibliothek Your knowledge hub WIEN

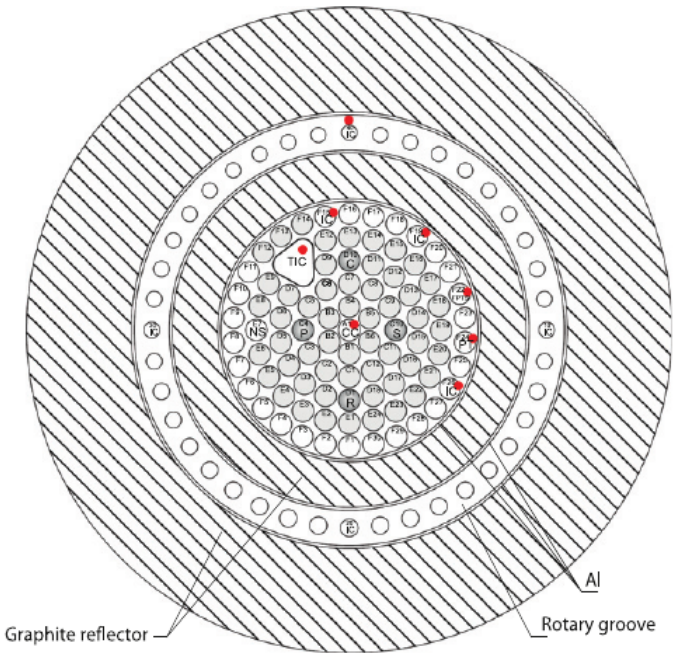


Figure 22: Modified horizontal JSI TRIGA reactor core cross section with the triangular irradiation channel on the upper left.[12]

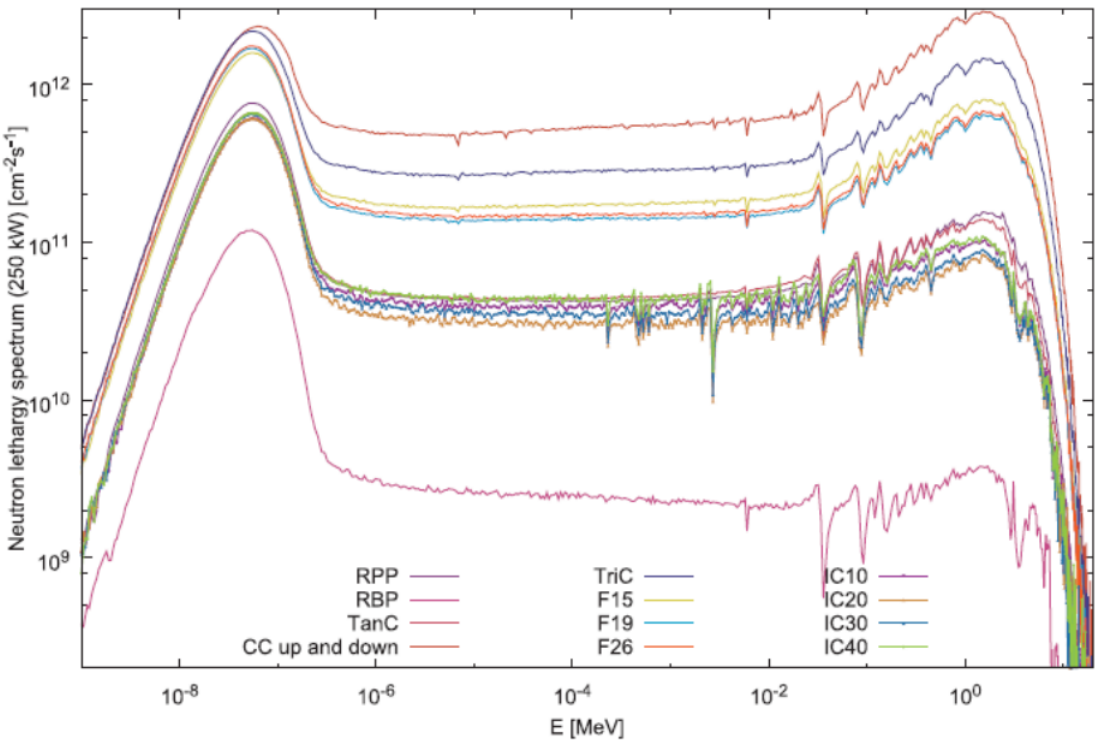


Figure 23: Spectrum of the Jožef Stefan Institute TRIGA reactor[13]. The Channel IC40 is the Ljubljana equivalent to Lazy Susan at the ATI.

Die approbierte gedruckte Originalversion dieser Diplomarbeit ist an der TU Wien Bibliothek verfügbar
The approved original version of this thesis is available in print at TU Wien Bibliothek.

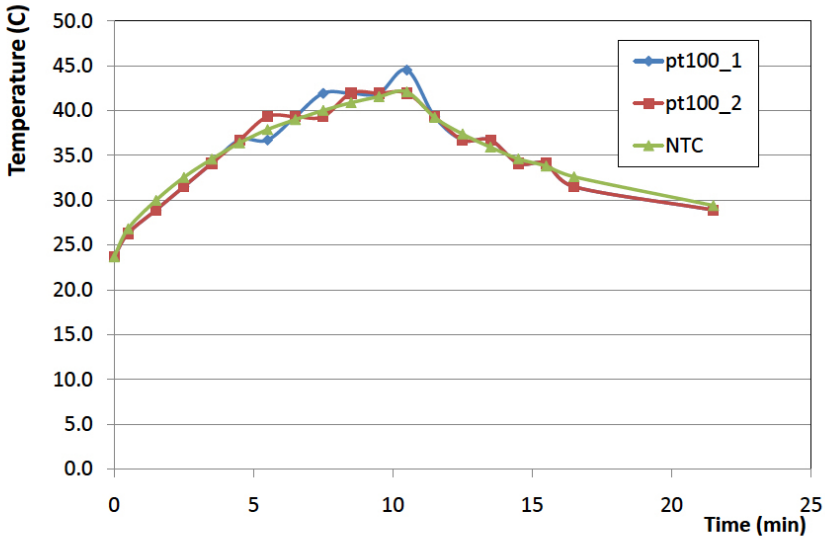


Figure 24: Temperature measurement at full reactor power. Taken from[28]

# 5 Sample irradiation for probe carrier material

Some preliminary practice for diode irradiation is to find useful probe carrier material in terms of neutron activation, practicability and stability. Stability and practicability can be neglected in this discussion. Therefore material selection in respect of neutron activation will be treated with notably diligence. Particular attention is paid to this, since the irradiated Si samples have to be cooled as quickly as possible after the neutron treatment. Therefore, the requirement on the probe carrier is a very short decay time and the lowest possible activation capability. Unfortunately, both the detector crescent and the probe carrier are more or less highly activated after the irradiation and have to decay before further handling is possible. The given limitation from the reactor is the aluminum powder of the LS cladding tube. aluminum is manageable after about half an hour. The next fixed constant is the Si wafer with given doping. The naked half moon can be handled within the decay time of aluminum. Now the task is to find a probe carrier material with as low as possible neutron activatability. Therefore no metals are desired and the lower the element number the better. Eight materials have been depicted. Before any material is allowed to enter the irradiation tubes a brief activation calculation is obligatory. (ATI reactor and radiation protection rule). The chemical compound can be extracted or investigated from the name and the calculation is done with the FRM II online tool[14]. An example of the calculation is given in 8.2.

[14] https://webapps.frm2.tum.de/intranet/activation/



Die approbierte gedruckte Originalversion dieser Diplomarbeit ist an der TU Wien Bibliothek verfügbar
The approved original version of this thesis is available in print at TU Wien Bibliothek.
TU Bibliothek Your knowledge hub WIEN

To extract useful data and to estimate the worst case activity, the samples are irradiated a whole reactor work day of 8 hours (performed 07.02.2020). Table 25 shows the selected materials, particular mass, dose rate, $\beta$ particle count and the activity of the samples about 30 min and 3 d after the irradiation.

| Nr. | | A1 | A2 | B1 | B2 | C1 | C2 | D | E |
|---|---|---|---|---|---|---|---|---|---|
| Name | | Delrin | Gelb | PEEK | PP | PET | FR4 | Birkenholz | Moosgummi |
| Masse (g) | | 2.3 | 1.9 | 2.5 | 1.3 | 2.2 | 2.9 | 1 | 0.2 |
| Dosisleistung (µSv) Kontakt | | 0.1 | 30 | 48 | 25 | | | 2.6 | 1.4 |
| β (counts/s) | | 80 | 8900 | 16500 | 38900 | | | 13000 | 5300 |
| Nuklid | HWZ (d) | Aktivität am 10.02.2020 in Bq | | | | | | | |
| Na-24 | 0.625 | 220 | 90400 | 97700 | 1200 | ? | ? | 2200 | 5000 |
| K-42 | 0.5 | | | 14300 | | | | 10100 | |
| Sc-46 | 83 | | | 3600 | | | 7500 | | |
| Ca-47 | 4.5 | | | 1500 | | | 2700 | | |
| Cr-51 | 27 | | | 2200 | 4000 | | 5000 | | |
| Zn-65 | 244 | | | | | | | | 9800 |
| Br-82 | 1.5 | 210 | 1300 | 630 | | | 9600000 | 4200 | 840 |
| Sb-122 | 2.7 | | | 1600 | 315000 | 350000 | | | |
| Sb-124 | 60 | | | | 17000 | 19000 | | | |
| La-140 | 1.7 | | | 1380 | | | | | 1200 |
| Sm-153 | 1.9 | | | 2000 | | | 72500 | | 1200 |

Figure 25: Probe carrier material activation study

Figure 26: TRIGA plastic test tubes. The one with the larger Diameter is for LS, the smaller one is for the pneumatic irradiation channel.

The samples were lowered into the reactor in PE plastic test tubes. To cover everything and estimate the max possible neutron activation, an empty tube (fig. 26) was irradiated for 8 hours and measured afterwards. The activity result is shown in figure 27.

Die approbierte gedruckte Originalversion dieser Diplomarbeit ist an der TU Wien Bibliothek verfügbar
The approved original version of this thesis is available in print at TU Wien Bibliothek.
TU Bibliothek Your knowledge hub WIEN

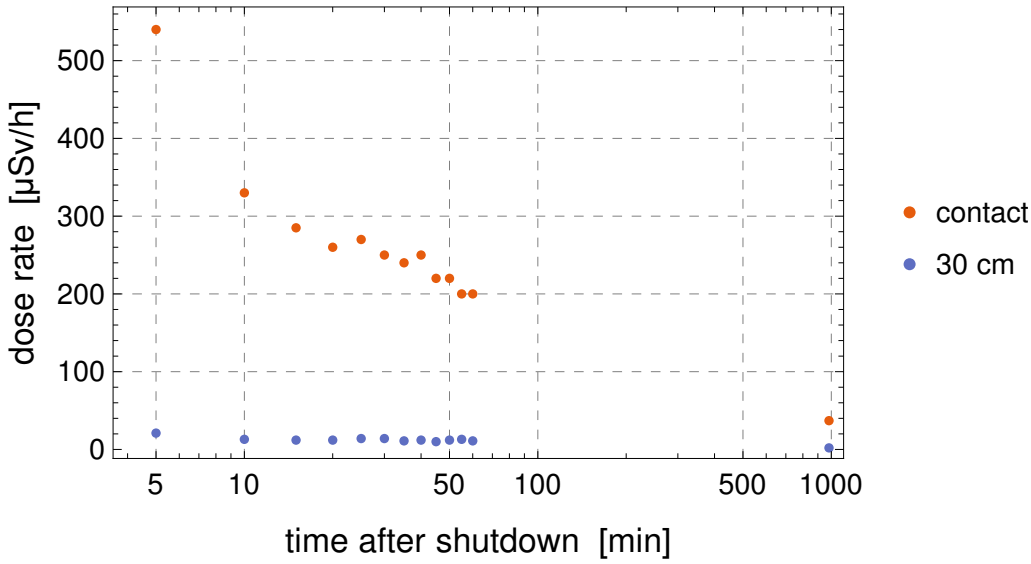


Figure 27: Activity result of the empty probe tube

# 6 Diode irradiation and measurement

This chapter is the practical main part of the thesis. At first I give a brief introduction about the used structures. Then the irradiation procedure at the ATI TRIGA Mark II Reactor is explained for further collaboration. The major component of this chapter is the analysis of the measurements and the calculation of the alpha factor. Moreover the frequency behavior of the diodes is examined.

## 6.1 Used half moons

HAMAMATSU CMS-6INCH-CUT OFFS W1T are the used structures for irradiation and reactor characterization. (Quick sidenote: W stands for wedge and T for tracker.) The four diode array with multiple Guard Rings (GR) was selected from the cut offs. The doping of the sensor and the test structures is p in n - Type. This means the top implantation is p - Type and the substrate is n - Type. A sketch of the layout is given in fig. 28 and a picture of the half moon in fig. 29.

The physical thickness of the structure is 320 µm and the active thickness of the structure is 300 µm. The area is 13.97 $mm^2$. With this dimensions the active volume of the diode is 4.191 $mm^3$. The capacitance at full depletion of non irradiated diodes is 5.4 pF. In this thesis 5 samples from two different Lot No. were used:

- Lot No. SWA63406 with Serial No. 30221541001**127**

and

- Lot No. SWA63346 with Serial Nos. 30221540800**711**, **712**, **713**, **715**



Die approbierte gedruckte Originalversion dieser Diplomarbeit ist an der TU Wien Bibliothek verfügbar
The approved original version of this thesis is available in print at TU Wien Bibliothek.
TU Bibliothek Your knowledge hub WIEN

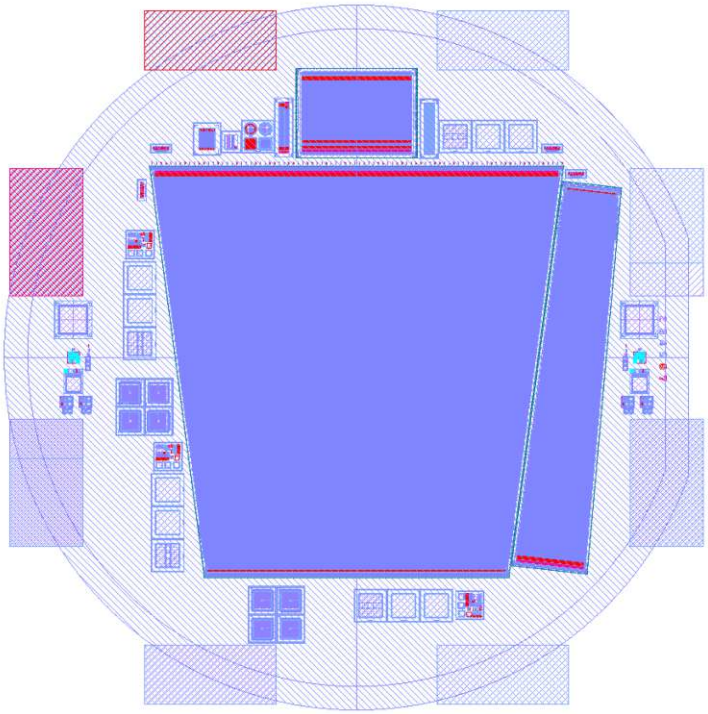

Figure 28: Sketch of the CMS-W1T wafer structure

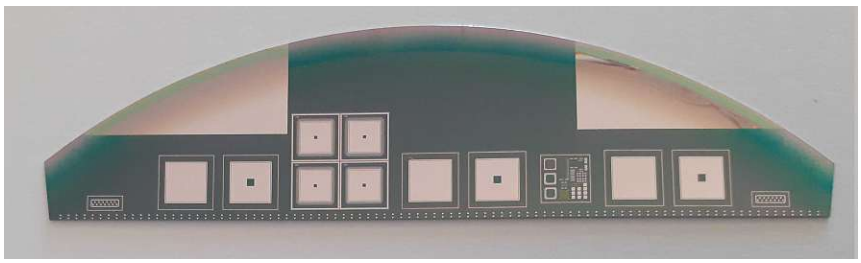

Figure 29: Picture of the used half moon with the four diode array

711, 712, 713 and 715 are the last 3 digits of the Serial No. of the same Lot. From now just the last three numbers are taken to identify the treated sample.

## 6.2 Half moon preparation

- select target fluence ($\phi_{eq}^{1\mathrm{MeV}}$)
- determine reactor power and irradiation time
- careful cleaning
- half moons sealed in blue dicing foil from Nitto as protection against scratches and bumps → helped to avoid scratches completely and was not activated (no further measures such as specimen holder required)
- instructed reactor team to careful handling and precise execution



Die approbierte gedruckte Originalversion dieser Diplomarbeit ist an der TU Wien Bibliothek verfügbar
The approved original version of this thesis is available in print at TU Wien Bibliothek.
TU Bibliothek Your knowledge hub WIEN

## 6.3 Irradiation

The five half moons were irradiated to the target fluences shown in Table 1. The irradiation time with selected reactor power is yellow highlighted. Fast and slow neutron radiation should be isotropic, so the alignment of the half moons in the sample tube is irrelevant. The loading procedure is to simply drop the plastic test tubes with the half moons into the LS beam pipes. After the target irradiation time/fluence was reached, the reactor was shut down and the test tubes were lifted via a manual winch. To reduce the relative error while insertion and extraction of the samples, the lower two fluences have been done by reduced reactor power (due to the short handling time at full reactor power). After the

| Probe | Fluenz | bei 250 kW | bei 25 kW | α [A/cm] | Lazy Susan |
|---|---|---|---|---|---|
| 127 | 5e13 | 1,8 min | 18 min | 5,699 e-17 | R4 |
| 715 | 1e14 | 3,6 min | 36 min | 5,675 e-17 | R2 |
| 713 | 5e14 | 18 min | 3 h | 5,594 e-17 | R4 |
| 712 | 1e15 | 36 min | 6 h | 5,509 e-17 | R2 |
| 711 | 1e16 | 6 h | - - - | 4,795 e-17 | R3 |

Table 1: Target fluences for half moon irradiation. The irradiation times with the reactor power for best handling of the probes is highlighted in yellow. The irradiation tubes used are shown in the last column. The penultimate row shows the corresponding current related damage rate $\alpha$.

reactor was shut down, the samples remained in the reactor tank overnight to decay and were placed in the freezer in the morning.

The annealing estimation is performed with the following assumptions:

| 250 kW | 25 kW |
|---|---|
| 18/36 + 2 min @ 40 °C | 18/36 + 2 min @ 30 °C |
| 5 min @ 30 °C | 3 min @ 25 °C |
| 1010 min @ 22 °C | 986 min @ 22 °C |

Table 2: Temperature history assumption in the LS beam tube during irradiation and after shutdown before cooling. The +2 min are the estimated time to fade from 40 °C to 30 °C.

Based on these temperature estimates, an equivalent annealing time at 60 degree C is calculated. The result is displayed in Table 1. The equivalent annealing time at 60 °C is in the range of 3.7 to 6.4 minutes for the four lower fluences. This is 4 to 8 percent of the standard annealing time.



Die approbierte gedruckte Originalversion dieser Diplomarbeit ist an der TU Wien Bibliothek verfügbar
The approved original version of this thesis is available in print at TU Wien Bibliothek.
TU Bibliothek Your knowledge hub WIEN

## 6.4 Measurements and annealing

The macroscopic properties of semiconductors change due to radiation induced microscopic defects. For more information see chapter 3. Initially n - Type doped substrate will become p - Type after severe irradiation. All measurements were taken at −20 °C. The CV measurements were performed at various frequencies between 500 Hz and 1 MHz.

### 6.4.1 Measurement setup

The wiring of the IV measurement setup is given in fig. 30. GR in the sketches is the outer Guard Ring of the diodes. The Source Measure Unit (SMU) Keithley 2410 and the Electrometer (EM) Keithley 6514 are the used devices.

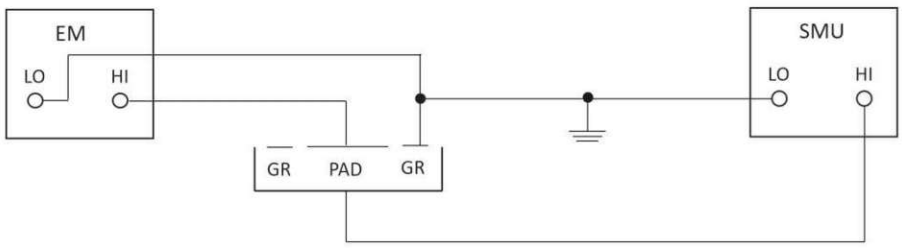


Figure 30: Sketch of the used IV measurement setup

The wiring of the CV measurement setup is given in fig. 31. The used devices for CV measurements are the SMU Keithley 2410, the EM Keithley 6514 and the LCR Meter Agilent E4980A.

### 6.4.2 Leakage current and alpha evaluation

The current vs voltage behavior of all 5 fluences and 0 min annealing is given in fig. 32. Consider the logarithmic scale of the vertical axis.

With the work done in [7], $\alpha$ is parameterized with

$$\alpha(T,t) = e^{-\frac{t}{\tau_I}} + \alpha_0 - \beta \cdot \ln\left(\frac{t}{t_0}\right) \tag{19}$$

Alpha for the irradiated samples is in the range of $\alpha(T,t) = 5.5 \cdot 10^{-17}$. The detailed values are calculated with the assumptions from Table 2 and listed in Table 3.

The description about the calculation of $\alpha(T,t)$ is given in chapter 8.3. Note the temperature dependence of $\alpha$ and eventually transform to a different temperature with Equation 9. The equivalent fluence of the reactor is calculated with the measured current



Die approbierte gedruckte Originalversion dieser Diplomarbeit ist an der TU Wien Bibliothek verfügbar
The approved original version of this thesis is available in print at TU Wien Bibliothek.
TU Bibliothek Your knowledge hub WIEN

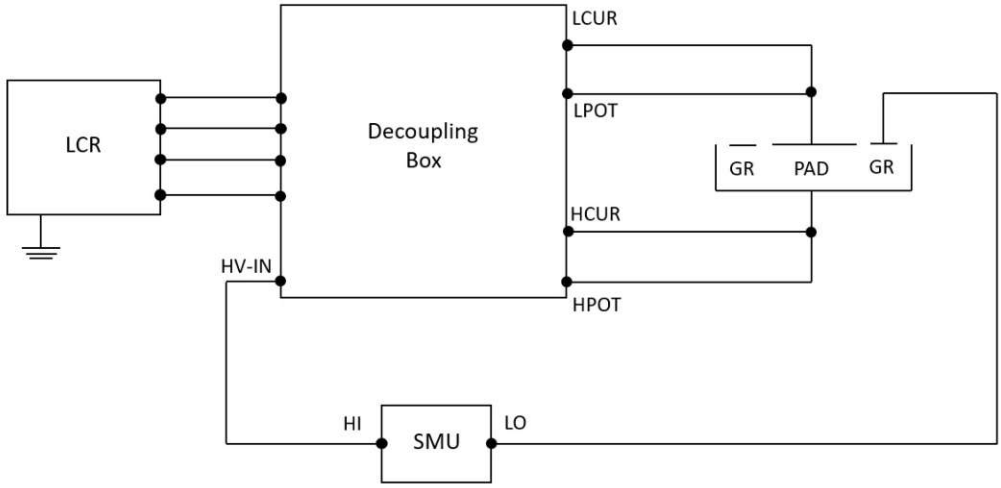


Figure 31: Sketch of the used CV measurement setup

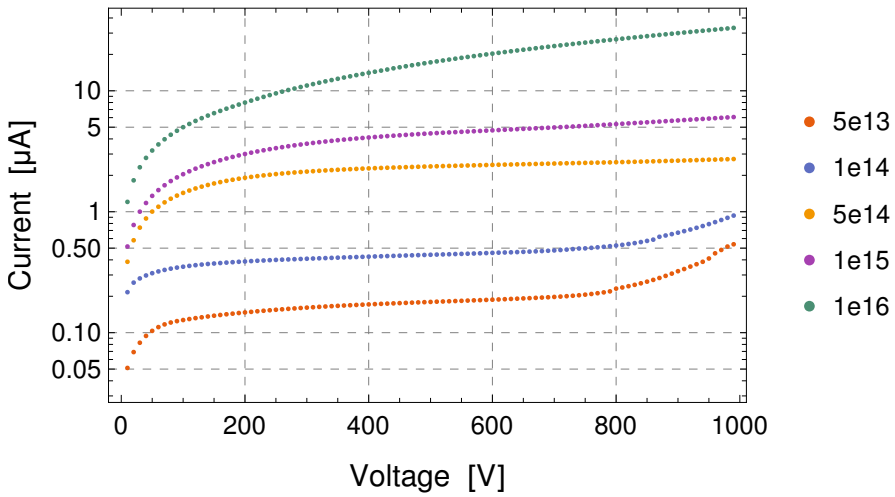


Figure 32: Current - voltage behavior of all 5 fluences and 0 min annealing with logarithmic scale of the vertical axis.

behavior and the calculated alpha value. Therefore Equation 17 is transformed to $\Phi_{eq}$ and evaluated. The result is given in Table 3. Since the 1e16 diode is not fully depletable beneath 1000 V the calculation does not make any sense and is ignored. The current related damage rate is the can be displayed as the slope of $\Delta I$ over $\phi_{eq}$. Therefore the current is taken at 600, 700, 800 and 900 Volt and plotted over all fluences. The green line in fig. 33 represents the fluence dependent linear increase of the leakage current.

Kappa is calculated with the following equation:

$$\kappa = \frac{\Phi_{eq}}{\Phi}. \tag{20}$$

The result with the fluences is given in Table 4. The values for the samples 1e14, 5e14



Die approbierte gedruckte Originalversion dieser Diplomarbeit ist an der TU Wien Bibliothek verfügbar
The approved original version of this thesis is available in print at TU Wien Bibliothek.
TU Bibliothek Your knowledge hub WIEN

| Probe | I bei 600 V [A] | $\Phi_{eq}$ $\left[\frac{n}{cm^2}\right]$ | $\alpha$ $\left[\frac{A}{cm}\right]$ |
|---|---|---|---|
| 127 | $1.25 \cdot 10^{-5}$ | $5.23 \cdot 10^{13}$ | $5.699 \cdot 10^{-17}$ |
| 715 | $2.82 \cdot 10^{-5}$ | $1.18 \cdot 10^{14}$ | $5.675 \cdot 10^{-17}$ |
| 713 | $1.42 \cdot 10^{-4}$ | $6.05 \cdot 10^{14}$ | $5.594 \cdot 10^{-17}$ |
| 712 | $2.78 \cdot 10^{-4}$ | $1.2 \cdot 10^{15}$ | $5.509 \cdot 10^{-17}$ |
| 711 | | | $4.795 \cdot 10^{-17}$ |

Table 3: The calculated equivalent fluence measured at 600 V and 20 °C

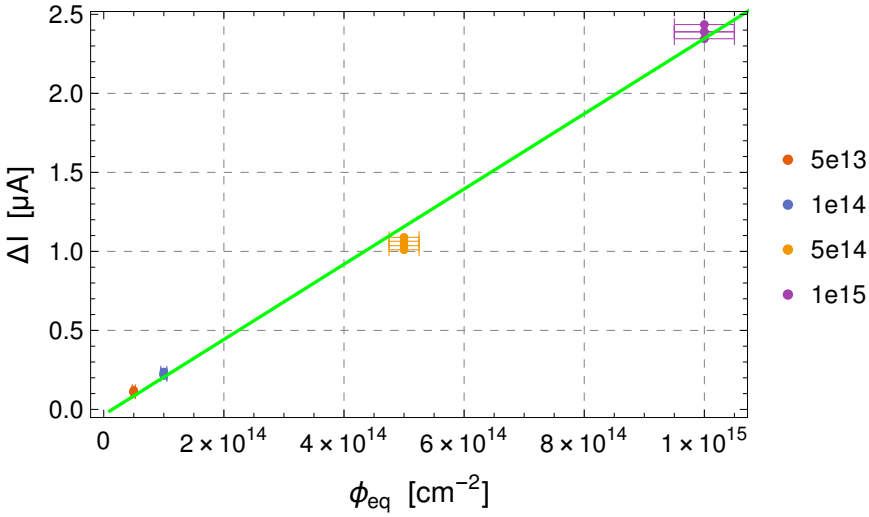


Figure 33: The proportionality factor $\alpha(T,t) = 5.5 \cdot 10^{-17}$ displayed as the slope of $\Delta I$ over $\phi_{eq}$. The errorbars represent the uncertainty in the measured fluence compared to the target fluence.

| Probe | $\Phi_{eq}$ $\left[\frac{n}{cm^2}\right]$ | $\Phi$ $\left[\frac{n}{cm^2}\right]$ | $\kappa$ |
|---|---|---|---|
| 127 | $5.23 \cdot 10^{13}$ | $5 \cdot 10^{13}$ | 0.95 |
| 715 | $1.18 \cdot 10^{14}$ | $1 \cdot 10^{14}$ | 0.84 |
| 713 | $6.05 \cdot 10^{14}$ | $5 \cdot 10^{14}$ | 0.82 |
| 712 | $1.2 \cdot 10^{15}$ | $1 \cdot 10^{15}$ | 0.83 |

Table 4: Result of the hardness factor $\kappa$ measurement calculation

and 1e15 agree well with the calculated value from section 4.1.2 for higher energies. 1e14 and 1e15 were irradiated at different reactor power but in the same LS tube. 5e13 and 5e14 were also irradiated in the same beam tube at different reactor power. $\kappa$ for the lower fluence deviates significantly from the calculated value. The deviation is probably rooted in the fact that the samples stayed in the reactor pool overnight. The post-decay has a greater effect on sensors irradiated with low fluence.

Fig. 34 shows the current behavior of the 5e14 sample in 10 min annealing steps. As clearly evident the leakage current decreases with increasing annealing time. All 5 fluences



Die approbierte gedruckte Originalversion dieser Diplomarbeit ist an der TU Wien Bibliothek verfügbar
The approved original version of this thesis is available in print at TU Wien Bibliothek.
TU Bibliothek WIEN Your knowledge hub

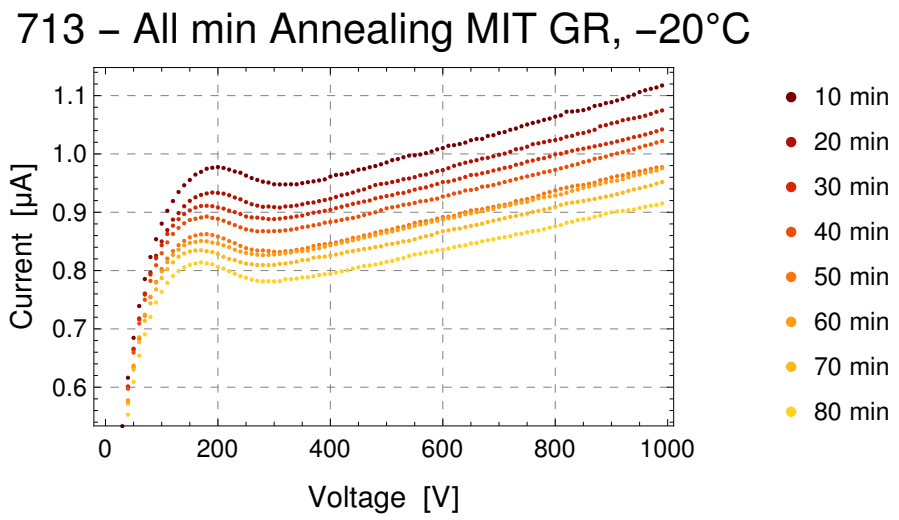


Figure 34: Annealing behavior of the sample irradiated to the fluence 5e14

show the same current - annealing behavior. The annealing behavior of the normalized leakage current at 600 V for all fluences is displayed in fig. 35. All measurements were taken at −20 °C.

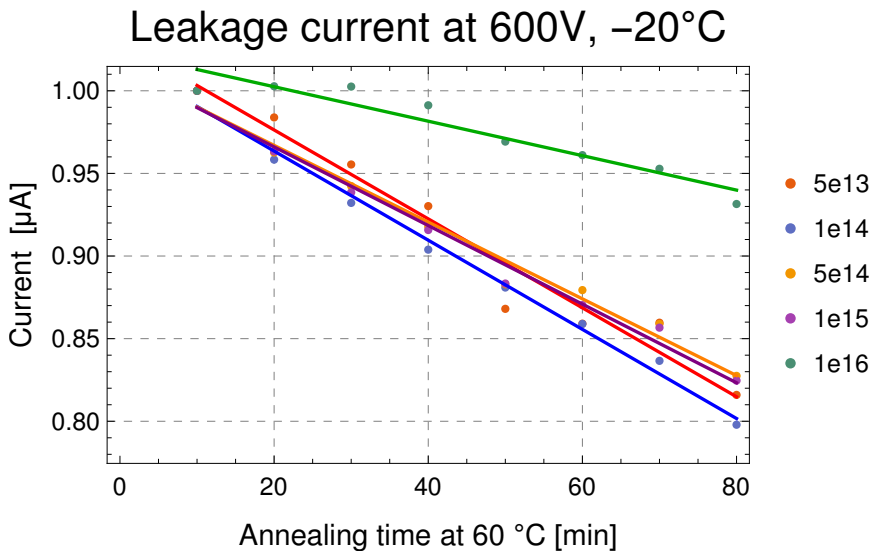


Figure 35: Logarithmic annealing behavior of the normalized leakage current for all fluences.

### 6.4.3 Capacitance behavior

In the literature, the capacitance study is usually carried out for the lower frequencies. As can be seen in fig. 36, the capacitance becomes a constant for higher frequencies. This behavior is visible for all fluences. Hence, higher frequencies are useless for diode characterization. The following analysis is only useful for 500 Hz and 1 kHz.

Fig. 37 shows the $\frac{1}{C^2}$ characteristics for the five samples with increasing fluence from



Die approbierte gedruckte Originalversion dieser Diplomarbeit ist an der TU Wien Bibliothek verfügbar
The approved original version of this thesis is available in print at TU Wien Bibliothek.
TU Bibliothek Your knowledge hub WIEN

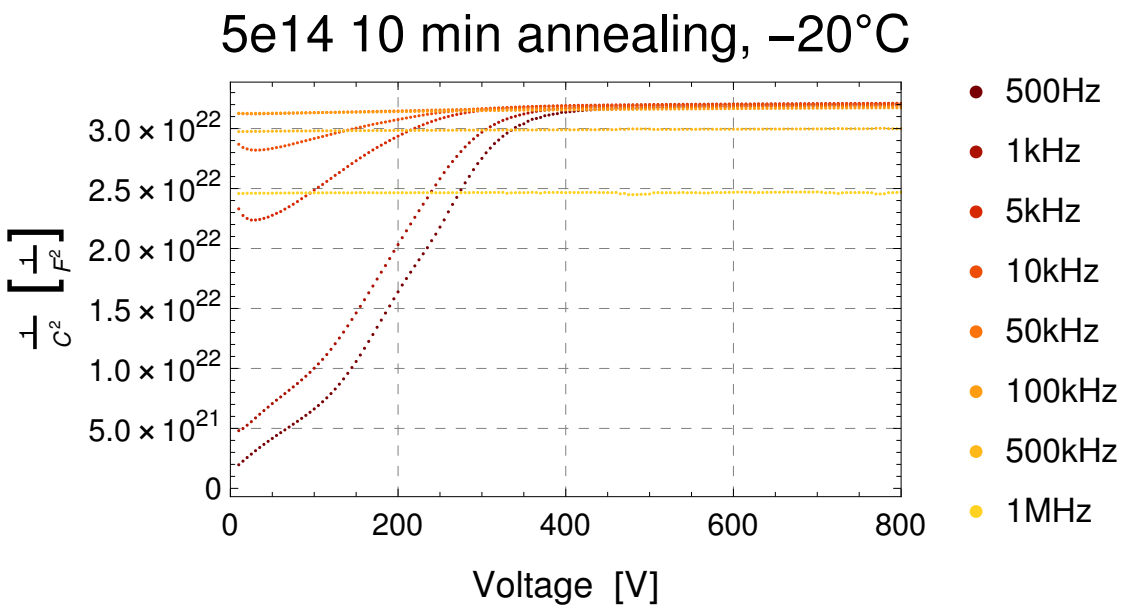


Figure 36: Frequency dependence of the capacitance of the 5e14 sample. Towards higher frequencies, the capacitance takes a constant value.

left to right. The measurement frequency was 500 Hz. The level at which the curves become a constant value is an indicator of full depletion. After type inversion, an increase in fluence leads to a steady donor creation and so to an increase in the full depletion voltage. Interesting is the "jump" in the 50 and 60 minutes annealing measurements. As

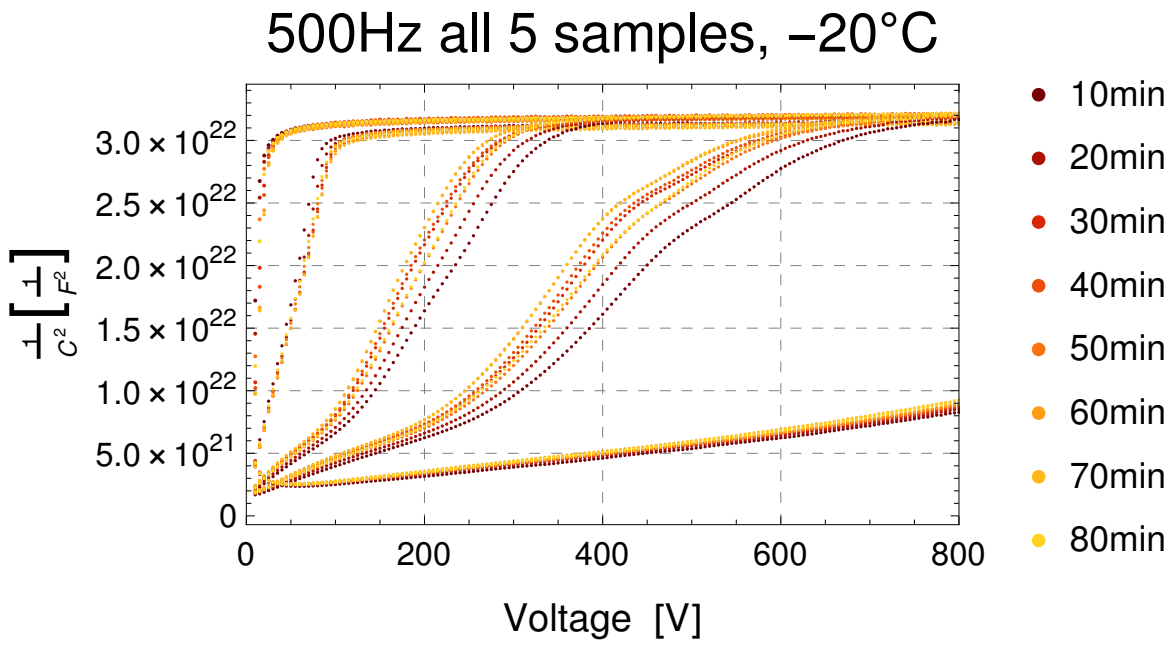


Figure 37: $\frac{1}{C^2}$ plot groups for the 5 samples with increasing fluecne from left to right. The different colors display the annealing behavior in 10 min steps. The measurement frequency was 500 Hz. Consider the color jump after 50 min annealing.

clearly visible, the lighter and darker measurements swap places. This effect occurs in



Die approbierte gedruckte Originalversion dieser Diplomarbeit ist an der TU Wien Bibliothek verfügbar
The approved original version of this thesis is available in print at TU Wien Bibliothek.
TU Bibliothek Your knowledge hub WIEN

all frequency measurements. In [29] the annealing behavior of the same structures were analyzed. According to [29] p.96, the change of the total capacitance of the full depleted sensors after irradiation is a result of the change in the dielectric constant of the bulk material. Unfortunately, no data are available in the literature. So the Si standard dielectric constant of 11.9 is taken for further calculations. The behavior of the full depletion voltage in 10 min annealing steps at 60 °C for all samples can be seen on a logarithmic scale in fig. 38.

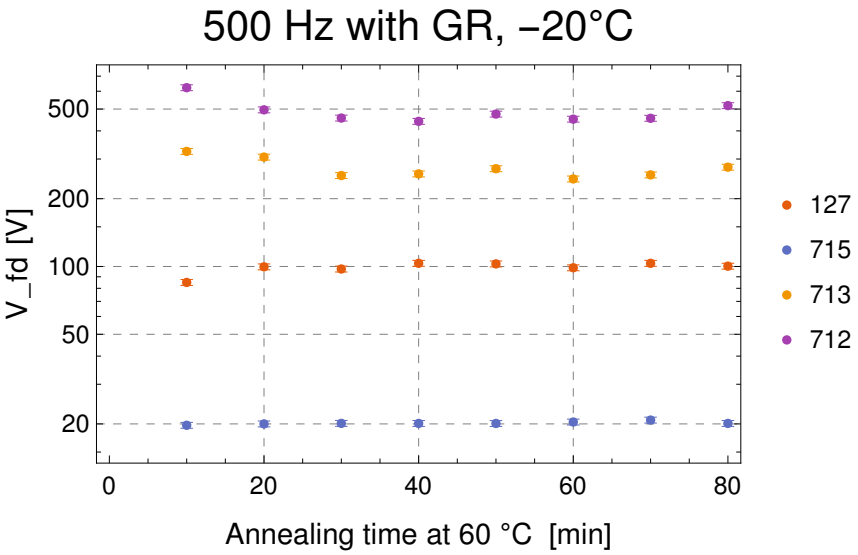


Figure 38: Logarithmic behavior of the $V_{fd}$ measured at 500 Hz. Between the measurements 10 min annealing steps at 60 °C were performed.

The full depletion voltage for the 5e13 sample is about 100 V. The $V_{fd}$ for the stronger irradiated 1e14 diode drops and increases significantly over 200 V for increasing fluence. Together with fig. 39 the type inversion is clearly evident. The parameters from Furgeri

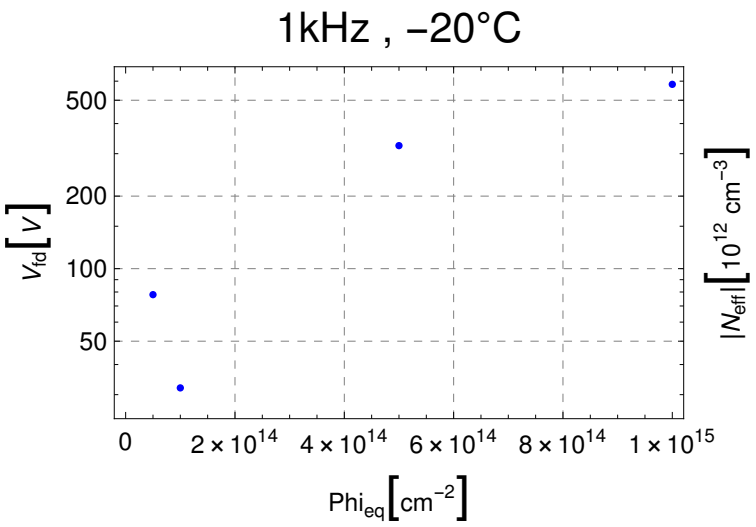


Figure 39: $V_{fd}$ for the measurement frequency of 1 kHz over the equivalent fluence. The dip on the lower left indicates the type inversion.

Die approbierte gedruckte Originalversion dieser Diplomarbeit ist an der TU Wien Bibliothek verfügbar
The approved original version of this thesis is available in print at TU Wien Bibliothek.
TU Bibliothek Your knowledge hub WIEN

Table 6.3 are confirmed again with this work.

### 6.4.4 Frequency behavior

This section briefly summarizes the frequency behavior of irradiated diodes. The $V_{fd}$increases 15 - 20 percent for decreasing frequency. This manner is mainly caused by resonance effects of defects. Fig. 40 to 42 show the capacitance and annealing behavior for higher frequencies. Interesting is the shift at higher voltages. This effect occurs for all fluences towards higher voltages. The capacitance for the 500 kHz and 1 MHz measurement is more or less constant and shows no voltage dependence. After the shift in the capacitance the samples with lower fluence and lower frequencies show only noisy behavior, as visible in fig. 40. This behavior is likely caused by micro-discharges[30]. At higher voltages, the local electric fields are strong enough to flash over.

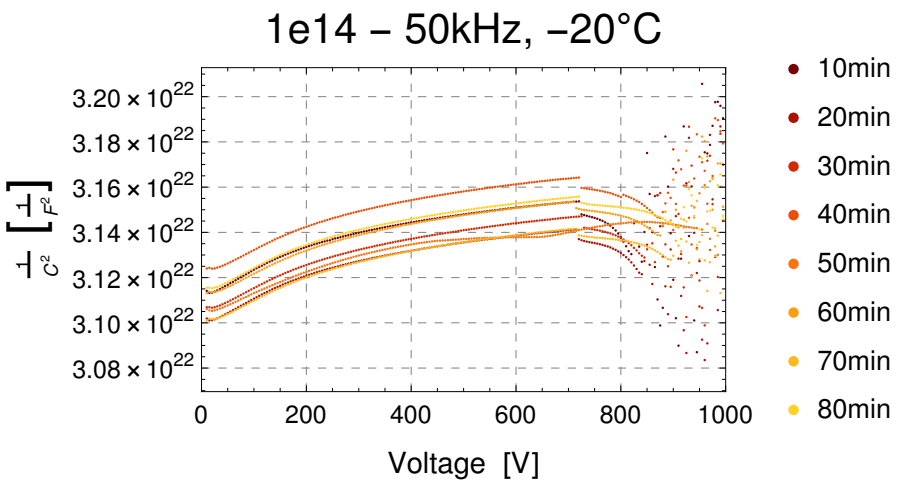


Figure 40: 1e14 50 kHz

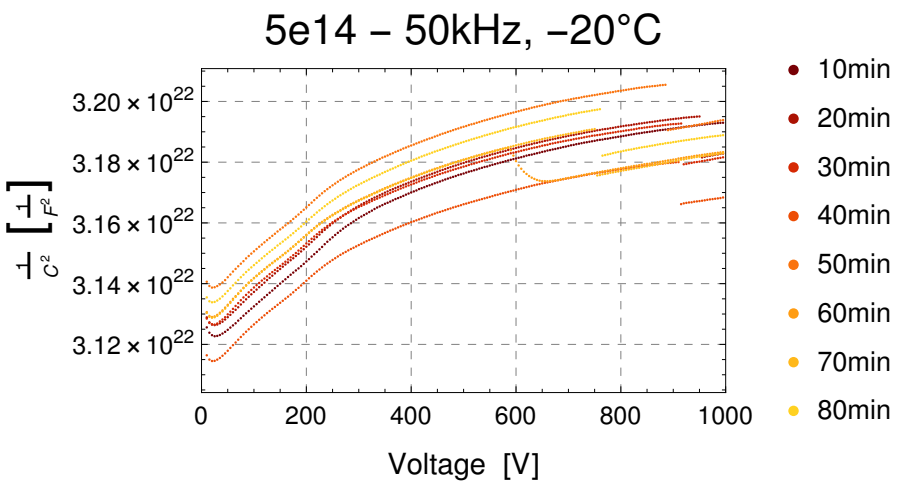


Figure 41: 5e14 50 kHz

Die approbierte gedruckte Originalversion dieser Diplomarbeit ist an der TU Wien Bibliothek verfügbar
The approved original version of this thesis is available in print at TU Wien Bibliothek.
TU Bibliothek Your knowledge hub WIEN

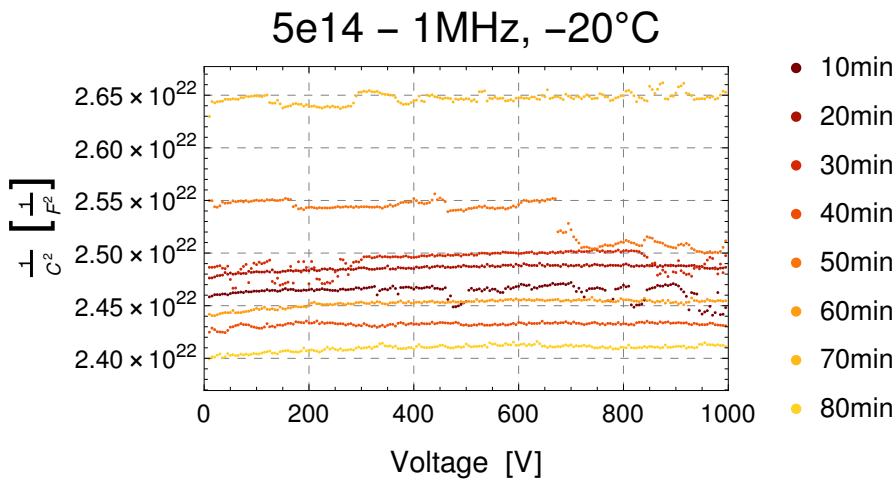


Figure 42: 5e14 1 MHz

# 7 Summary and Outlook

The current CMS detectors are not appropriate for fluences higher than 5e15. This is why the HL-LHC and future colliders require improvements in detector radiation hardness. The main problem with highly irradiated silicon semiconductor detectors is the high voltage that is required for full depletion. High voltages imply high electrical fields, which in turn require geometrical optimizations. Radiation hardening studies have been well discussed in the literature so far. In addition section 3.5 suggests to use dopant atoms with low or vanishing neutron cross section to reduce neutron capture in detector segments with high expected neutron flux. With the sample carrier irradiation study, Delrin is the most suitable plastic in terms of neutron activation. Since the reactor team has used paper tissue and cotton as shock protection for years, a special probe carrier is actually not required. Unfortunately, the temperature in the irradiation tube could not be logged, which would have had a positive effect on the alpha calculation. This fact can be attributed to the reactor and radiation protection head.

## 7.1 Reactor fluence characterization and calculation for future irradiations

The total neutron flux in the LS beam tube of the TRIGA reactor of ATI is $3,69 \pm 0,31 \cdot 10^{12}\ \frac{neutrons}{cm^2 \cdot s}$. The 1 MeV equivalent fluence is calculated with Eq. 17. In the course of this thesis the hardness factor $\kappa$ was measured as well as calculated. The calculated value was obtained with Eq. 18 and integrated to $\kappa = 0.79$. The measured value was extracted from leakage current measurements and yields to 0.83. This is a 5 % deviation from measurement to calculation.

How to calculate the 1 MeV equivalent fluence for future irradiations:

Determine the desired 1 MeV target fluence $\phi_{eq}^{1\,\mathrm{MeV}}$. Use formula 20 and divide by $\kappa$. If lower fluences are wanted, reduce the reactor power to reduce the relative error introduced



Die approbierte gedruckte Originalversion dieser Diplomarbeit ist an der TU Wien Bibliothek verfügbar
The approved original version of this thesis is available in print at TU Wien Bibliothek.
TU Bibliothek Your knowledge hub WIEN

due to he short handling time. Calculate the irradiation time with the given neutron flux at the corresponding reactor power.

Die approbierte gedruckte Originalversion dieser Diplomarbeit ist an der TU Wien Bibliothek verfügbar
The approved original version of this thesis is available in print at TU Wien Bibliothek.
TU WIEN Bibliothek Your knowledge hub

# 8 Appendix

## 8.1 ATI Irradiation Procedure Manual

The following list provides an overview of the tasks to be performed for irradiations at the ATI:

- notification at the head of reactor/ATI
- estimate the expected activation of the sample
- pack the samples to protect against damage while dropping into the reactor
- calculate irradiation time and reactor power for desired fluence
- take care of coolant after irradiation
- radioactive release measurement from head of radiation protection
- transportation plan (eventually with coolant)
- carefully log time (for annealing history treatment)

## 8.2 Activation Calculation of PET

In the following the calculated activation result of PET is given. The calculation was performed with the FRM II online tool mentioned already in chapter 5.

Die approbierte gedruckte Originalversion dieser Diplomarbeit ist an der TU Wien Bibliothek verfügbar
The approved original version of this thesis is available in print at TU Wien Bibliothek.
TU WIEN Bibliothek Your knowledge hub

Die approbierte gedruckte Originalversion dieser Diplomarbeit ist an der TU Wien Bibliothek verfügbar
The approved original version of this thesis is available in print at TU Wien Bibliothek.
TU WIEN Bibliothek Your knowledge hub

**Activation Results**

Formula: C10H8O4
Mass: 2.2 g
Instrument: Manual
Flux: 3.7e+12 n/cm²s Cd ratio: 2 fast ratio: 2
Exposure time: 8 h
Decay time (using sum formula on mass specific limit): 1.0 h
Decay time (using sum formula on activity limit): 0.0 h
Over release limits
Over 10% of release limit

| | | | | | | | | | Activity (Bq) | | | |
|---|---|---|---|---|---|---|---|---|---|---|---|---|
| Daughter | reaction | mode | limit (Bq/g) | limit (Bq/g) 18 | limit2 (Bq) | limit2 (Bq) 18 | limit3 (Bq/g) | T1/2 | A@0.0 h | A@1.0 h | A@24.0 h | A@14.0 d |
| C-11 | n,2n | B+ | 10 | 10 | 1e+06 | 1e+06 | 10 | 20.3 m | 53 | 6.84 | < 1E-6 | < 1E-6 |
| C-14 | act | B- | 80 | 1 | 1e+07 | 1e+07 | 1e+04 | 5736 y | 0.618 | 0.618 | 0.618 | 0.618 |
| H-3 | act | B- | 1e+03 | 100 | 1e+09 | 1e+09 | 1e+06 | 12.346 y | 0.506 | 0.506 | 0.506 | 0.505 |
| N-16 | n,p | not av. | --- | --- | --- | --- | --- | 7.14 s | 9.67e+05 | < 1E-6 | < 1E-6 | < 1E-6 |
| O-15 | n,2n | B+ | 100 | 100 | 1e+09 | 1e+09 | 100 | 122 s | 27 | < 1E-6 | < 1E-6 | < 1E-6 |
| C-14 | n,a | B- | 80 | 1 | 1e+07 | 1e+07 | 1e+04 | 5736 y | 0.946 | 0.946 | 0.946 | 0.946 |
| N-17 | n,p | not av. | --- | --- | --- | --- | --- | 4.17 s | 157 | < 1E-6 | < 1E-6 | < 1E-6 |
| O-19 | act | B-, G | --- | --- | 1e+05 | 1e+04 | --- | 27.1 s | 1.11e+05 | < 1E-6 | < 1E-6 | < 1E-6 |
| | | | | | | | | total | 1.08e+06 | 8.91 | 2.07 | 2.07 |
| | | | | | | | | Dose (µSv/h) | 0.06 | < 1E-6 | < 1E-6 | < 1E-6 |
| | | | | | | | | Dose (0.0 cm Pb) | 0.06 | < 1E-6 | < 1E-6 | < 1E-6 |

| | | | | | | | | Activity (Bq) | | | | |
|---|---|---|---|---|---|---|---|---|---|---|---|---|
| r | reaction | mode | limit (Bq/g) | limit (Bq/g) 18 | limit2 (Bq) | limit2 (Bq) 18 | limit3 (Bq/g) | T1/2 | A@0.0 h | A@0.0 h | A@0.0 h | A@0.4 h | A@0.4 h |
| | n,2n | B+ | 10 | 10 | 1e+06 | 1e+06 | 10 | 20.3 m | 53 | 48.9 | 48.8 | 22 | 21.8 |
| | act | B- | 80 | 1 | 1e+07 | 1e+07 | 1e+04 | 5736 y | 0.618 | 0.618 | 0.618 | 0.618 | 0.618 |
| | act | B- | 1e+03 | 100 | 1e+09 | 1e+09 | 1e+06 | 12.346 y | 0.506 | 0.506 | 0.506 | 0.506 | 0.506 |
| | n,p | not av. | --- | --- | --- | --- | --- | 7.14 s | 9.67e+05 | 0.971 | 0.73 | < 1E-6 | < 1E-6 |
| | n,2n | B+ | 100 | 100 | 1e+09 | 1e+09 | 100 | 122 s | 27 | 12 | 11.8 | 0.00411 | 0.00376 |
| | n,a | B- | 80 | 1 | 1e+07 | 1e+07 | 1e+04 | 5736 y | 0.946 | 0.946 | 0.946 | 0.946 | 0.946 |
| | n,p | not av. | --- | --- | --- | --- | --- | 4.17 s | 157 | < 1E-6 | < 1E-6 | < 1E-6 | < 1E-6 |
| | act | B-, G | --- | --- | 1e+05 | 1e+04 | --- | 27.1 s | 1.11e+05 | 2.91e+03 | 2.7e+03 | < 1E-6 | < 1E-6 |
| | | | | | | | | total | 1.08e+06 | 2.97e+03 | 2.76e+03 | 24.1 | 23.9 |
| | | | | | | | | Dose (µSv/h) | 0.06 | 0.002 | 0.001 | < 1E-6 | < 1E-6 |
| | | | | | | | | Dose (0.0 cm Pb) | 0.06 | 0.002 | 0.001 | < 1E-6 | < 1E-6 |

limit: The limit (mass specific activity) for release from the control as radioactive substance(Freigabegrenzwert)
limit2: The limit (absolute activity) for handling a radioactive substance without license (Freigrenze)
limit: The limit (mass specific activity) for release from the control as radioactive substance(Freigabegrenzwert)
limit2: The limit (absolute activity) for handling a radioactive substance without license (Freigrenze)
limit3: The limit (mass specific activity) for handling a radioactive substance without license (Freigrenze)
Currently the highest value of these limits is used for returning a sample to users.

The limit values presented here are prepared with best knowlegde, but the official source is always **Strahlenschutzverordnung.**

The decay time is estimated only on the basis of the mass-specific limits.

Dose values are calculated for 50 cm distance with point source geometry. The values should provide a hint for necessary shielding, but don`t forget to measure before handling irradiated samples.

The shielding calculation does not take buildup into account and uses the `Broad Beam Conditions approximation.

Die approbierte gedruckte Originalversion dieser Diplomarbeit ist an der TU Wien Bibliothek verfügbar
The approved original version of this thesis is available in print at TU Wien Bibliothek.
TU WIEN Bibliothek Your knowledge hub

## 8.3 Annealing Calculation

There is an online tool to quickly calculate the $\alpha$ value from a simple time and temperature history: `https://annealing.cms-ka.fzk.de`. A more detailed elaboration of the formula and constants is given in [31] 4.2. Extensive histories and files cannot be processed with the online tool. During the course of this thesis I wrote a Fortran and a more reliable Mathematica program that calculate the $\alpha$ value from the temperature and time history of the sample. The data are read in from a 2-column file.

Another program to handle the Hamburg model, to calculate the effective doping and treat annealing can be found at the CERN gitlab repository: `https://gitlab.cern.ch/atlas/athena/tree/master/InnerDetector/InDetCalibAlgs/PixelCalibAlgs/RadDamage/HamburgModel`.

### 8.3.1 Mathematica code

The program prints the final alpha value, the equivalent $t_{60}$ time to reach this alpha value and two plots as pictured in fig. 43. If wanted the two plots can also be exported to a file.

```
(*  only constants  *)
al = 1.23*10^-17;     (*  A/cm *)
b = 3.07*10^-18;   (*  A/cm *)
c1 = -8.9*10^-17;    (*  A/cm *)
c2 = 4.6*10^-14;    (*  AK/cm *)
k0 = 1.2*10^13;     (* 1/s *)
El = 1.11;   (*  eV  *)
kB = 8.62*10^-5;    (*  eV/K  *)
(*  temparature dependent functions \
tau und A0 *)
tau[x_] := Exp[((12.9*10^3)/x) - 34.1]     (* min *)
A0[x_] := c1 + c2*(1/x)     (*  A/cm *)
alphax[x_] :=
 al*Exp[-(s[[x]]/tau[T[[x]]])] + A0[T[[x]]] -
  b*Log[s[[x]]]     (*  Alpha as function *)
(*  function for \
plotting  *)
TwoAxisListPlot[{f_, g_}, opts___] :=
 Module[{fgraph, ggraph, frange, grange, fticks,
   gticks}, {fgraph, ggraph} =
   MapIndexed[
    ListPlot[#, Axes -> True, PlotStyle -> ColorData[1][#2[[1]]],
```



Die approbierte gedruckte Originalversion dieser Diplomarbeit ist an der TU Wien Bibliothek verfügbar
The approved original version of this thesis is available in print at TU Wien Bibliothek.
TU Bibliothek Your knowledge hub WIEN

```
      opts] &, {f, g}]; {frange,
    grange} = (PlotRange /. AbsoluteOptions[#, PlotRange])[[
      2]] & /@ {fgraph, ggraph};
  fticks = N@FindDivisions[frange, 5];
  gticks =
   Quiet@Transpose@{fticks,
      ToString[NumberForm[#, 2], StandardForm] & /@
       Rescale[fticks, frange, grange]};
  Show[fgraph,
   ggraph /.
    Graphics[graph_, s___] :>
     Graphics[
      GeometricTransformation[graph,
       RescalingTransform[{{0, 1}, grange}, {{0, 1}, frange}]], s],
   Axes -> False, Frame -> True,
   FrameStyle -> {ColorData[1] /@ {1, 2}, {Automatic, Automatic}},
   FrameTicks -> {{fticks, gticks}, {Automatic, Automatic}}]]


(*   2-column file with time and Temp   *)
input = Import["/inputfilepath/filename"];
s = input [[1 ;;, 1]];     (*   time   *)
T =
 input[[1 ;;, 2]] +
  273.15;   (*   +273.15  if value in \[Degree]C , otherwise K   *)

yroot = y /.
  FindRoot[{(al*Exp[-(y/tau[T[[2]]])] + A0[T[[2]]] -
       b*Log[y]) == (al*Exp[-(s[[1]]/tau[T[[1]]])] + A0[T[[1]]] -
       b*Log[s[[1]]])}, {y, 10^-15}, PrecisionGoal -> 20,
   AccuracyGoal -> 20];
Quiet[Table[
   yneu =
    y /. FindRoot[{(al*Exp[-(y/tau[T[[i + 1]]])] + A0[T[[i + 1]]] -
          b*Log[y]) == (al*Exp[-((yroot + s[[i]])/tau[T[[i]]])] +
          A0[T[[i]]] - b*Log[(yroot + s[[i]])])}, {y, 10^-15},
      PrecisionGoal -> 20, AccuracyGoal -> 20];
   yroot = yneu,
   {i, 2, (Length[T] - 1)}]];
yliste = Insert[%, %%,
```

Die approbierte gedruckte Originalversion dieser Diplomarbeit ist an der TU Wien Bibliothek verfügbar
The approved original version of this thesis is available in print at TU Wien Bibliothek.
TU Bibliothek Your knowledge hub WIEN

```
  1];   (*  all y in a list *)
(*  pringt finalalpha *)
finalalpha =
 al*Exp[-((yroot + s[[Length[T]]])/tau[T[[Length[T]]]])] +
  A0[T[[Length[T]]]] - b*Log[(yroot + s[[Length[T]]])]

alphax[1];     (*  first Element *)
alphafast =
 Table[al*Exp[-((yliste[[i]] + s[[i + 1]])/tau[T[[i + 1]]])] +
   A0[T[[i + 1]]] - b*Log[(yliste[[i]] + s[[i + 1]])], {i,
   1, (Length[T] - 1)}];
alphaliste = Insert[alphafast, alphax[1], 1];

(*  t_60 = y60 over running Annealing *)
y60 = Quiet[
   Table[y /.
     FindRoot[{(al*Exp[-(y/tau[333])] + A0[333] -
          b*Log[y]) == (alphaliste[[i]])}, {y, 10^-15},
      AccuracyGoal -> 18, PrecisionGoal -> 18], {i,
     1, (Length[T])}]];
Last[y60]     (*  print equivalent t_60 time *)

TwoAxisListPlot[{alphaliste, y60}, {Frame -> True,
  PlotLabel -> "Plot Label", PlotRange -> All, Joined -> True,
  PlotMarkers -> {Automatic, Small}, ImageSize -> Large,
  FrameLabel -> {{"alpha [A/cm]", "t_60 [min]"}, {"duration [min]",
     ""}}, BaseStyle -> {FontSize -> 16}}]
(*   Export["/outfilepath/filename",%,ImageResolution\[Rule]600]   *)
\
TwoAxisListPlot[{T, y60}, {Frame -> True, PlotLabel -> "Plot Label",
  PlotRange -> All, Joined -> True, PlotMarkers -> {Automatic, Small},
   ImageSize -> Large,
  FrameLabel -> {{"Temperatur [K]", "t_60 [min]"}, {"duration [min]",
     ""}}, BaseStyle -> {FontSize -> 16}}]
(*   Export["/outfilepath/filename",%,ImageResolution\[Rule]600]   *)
```

### 8.3.2 Fortran code

The program calculates $\alpha$ and displays the corresponding annealing durations for 60 °C and 22 °C. The default input file is "werte.dat". To run the program in Linux, type "gfortran annealing.f95" into the shell prompt. Then run "./a.out".

Die approbierte gedruckte Originalversion dieser Diplomarbeit ist an der TU Wien Bibliothek verfügbar
The approved original version of this thesis is available in print at TU Wien Bibliothek.
TU Bibliothek Your knowledge hub WIEN

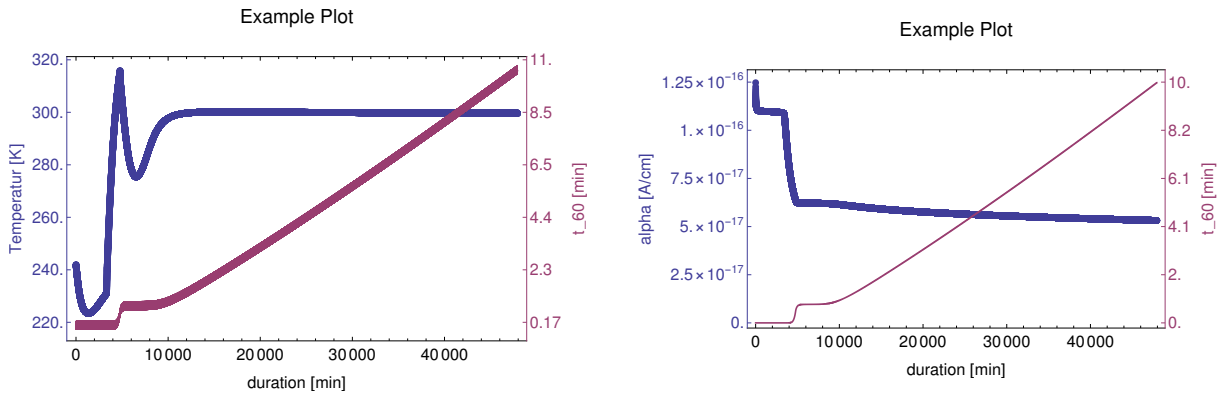


Figure 43: Mathematica example plot of the annealing history of sensors sent to and irradiated at RINSC

```
program Annealing
    implicit none

        double precision :: a        !   Alpha dependent from time (min)
                                         and Temparature (°C)
        double precision :: time, Temp
        double precision, parameter :: al = 1.23d-17, b = 3.07d-18
        double precision :: a0, tl, tvor
        double precision :: j, x, y, h                !   help variables
        integer ::  IO

a = 0d0
tvor = 0d0

!   open the existing file werte.dat
    open(1,file="werte.dat",status='old',IOstat=IO)
    write(*,*) "werte.dat:"
!   read the file
    do
        read(1,*,IOstat=IO)  time, Temp
        write(*,*) time, Temp, ". . . read from file"

        if (IO > 0d0)  then
             write(*,*) "file error ; please 2-column file with time in (min)
                         and Temparature in (°C)"
             stop
        else if (IO < 0d0) then
            write(*,*)
```



Die approbierte gedruckte Originalversion dieser Diplomarbeit ist an der TU Wien Bibliothek verfügbar
The approved original version of this thesis is available in print at TU Wien Bibliothek.
TU Bibliothek Your knowledge hub WIEN

```
            write(*,*) "EOF"
            exit
        else
            time = time - tvor
            write(*,*) time, Temp, ". . . calculated"
            Temp = Temp + 273.15d0


            a = a + al*exp(-time/tl(Temp)) + a0(Temp) - b*log(time)


             write(*,*) a
            tvor = time
        end if
    end do

    close(1)
    write(*,*) "file successfully read"
    write(*,*)


    write(*,*) "a0 =", a0(Temp)
    write(*,*) "tl =", tl(Temp)
    write(*,*) "Alpha =", a,"A/cm"          !  Ausgabe Alpha

!------------------------ 60°C Annealing Äquivalent
Temp = 333.15d0  ! (K) . . . = 60°C
j = 0d0
x = 0d0
y = 0d0

    do
            y = a-x
            j = j + 0.001d0
            x = al*exp(-j/tl(Temp)) + a0(Temp) - b*log(j)
           !write(*,*) a,x,y
        if (abs (y) < 1d-20) then
            write(*,*)
!           write(*,*) a,x,j
            exit
```

Die approbierte gedruckte Originalversion dieser Diplomarbeit ist an der TU Wien Bibliothek verfügbar
The approved original version of this thesis is available in print at TU Wien Bibliothek.
TU WIEN Bibliothek Your knowledge hub

```
        end if
    end do
    write(*,*) "This corresponds to an annealing time of",j," Min at 60°C"

!------------------------ 22°C Annealing Äquivalent
Temp = 295.15d0  ! (K) . . . = 22°C
h = 0d0
x = 0d0
y = 0d0

    do
            y = a-x
            h = h + 0.001d0
            x = al*exp(-h/tl(Temp)) + a0(Temp) - b*log(h)

        if (abs (y) < 1d-20) then
            write(*,*)
!           write(*,*) a,x,h
            exit
        end if
    end do
    write(*,*) "This corresponds to an annealing time of", h, "Min at 22°C"
    write(*,*)

end program


!------------------------


double precision function a0(Temp)
    implicit none
        double precision :: Temp
        double precision, parameter :: c1 = -8.9d-17, c2 = 4.6d-14

    a0  = c1 + c2 * (1./Temp)

end function a0

!------------------------
```

Die approbierte gedruckte Originalversion dieser Diplomarbeit ist an der TU Wien Bibliothek verfügbar
The approved original version of this thesis is available in print at TU Wien Bibliothek.
TU Bibliothek Your knowledge hub WIEN

```
double precision function tl(Temp)
    implicit none
        double precision :: Temp
        double precision, parameter :: k0 = 1.2d13, E = 1.11d0, kB = 8.62d-5

    tl  = 1d0/(k0*exp(-E/(kB*Temp)))

end function tl
```

Die approbierte gedruckte Originalversion dieser Diplomarbeit ist an der TU Wien Bibliothek verfügbar
The approved original version of this thesis is available in print at TU Wien Bibliothek.
TU WIEN Bibliothek Your knowledge hub

# References


[1] CERN. The accelerator complex. Technical report. [Online; accessed 27-May-2021].

[2] CERN. Project Schedule. Technical report. [Online; accessed 27-May-2021].

[3] Vidal X and Manzano R. Luminosity - Taking a closer look at LHC. Technical report. [Online; accessed 27-May-2021].

[4] Curras E, Mannelli M, Moll M, Nourbakhsh S, Steinbrueck G, and Vila I. Radiation hardness study of Silicon Detectors for the CMS High Granularity Calorimeter (HGCAL). Technical report, 2017.

[5] Bruning O and Rossi L. High-luminosity Large Hadron Collider. Technical report, 2020.

[6] Cubdri V. World irradiation facilites for silicon detectors. *The 23rd International Workshop on Vertex Detectors*, 2014.

[7] Moll M. *Radiation Damage in Silicon Particle Detectors - microscopic defects and macroscopic properties -*. PhD thesis, Universität Hamburg, 1999.

[8] Kasap S and Capper P. *Springer Handbook of Electronic and Photonic Materials.* Springer Verlag, 2017.

[9] Hönniger F. *Radiation Damage in Silicon - Defect Analysis and Detector Properties.* PhD thesis, Universität Hamburg, 2007.

[10] Villa M. Reaktorphysik. AIAU 98402, 2008.

[11] Kolanoski H and Wermes N. *Teilchendetektoren, Grundlagen und Anwendungen.* Springer Verlag, 2015.

[12] Junkes A. *Influence of radiation indued defects clusters on silicon particle detectors.* PhD thesis, Universität Hamburg, 2011.

[13] Bergauer T. Private Communication, June, 2021.

[14] König A. *Planar Silicon Strip Sensors for the CMS Phase-2 Upgrade.* PhD thesis, Technische Universität Wien, 2017.

[15] Lindström G, Moll M, Kuhnke M, and E. Fretwurst. RADIATION HARDNESS OF SILICON DETECTORS FOR APPLICATIONS IN HIGH-ENERGY PHYSICS EXPERIMENTS. *Journal of Optoerlectronics and Advanced Materials Vol. 2, No.5, 2000, p.575-588*, 2000.



Die approbierte gedruckte Originalversion dieser Diplomarbeit ist an der TU Wien Bibliothek verfügbar
The approved original version of this thesis is available in print at TU Wien Bibliothek.
TU Bibliothek WIEN Your knowledge hub

[16] Moll M, Fretwurst E, and Lindström G. Investigation on the improved radiation hardness of silicon detectors with high oxygen concentration CERN Project RD48 (The ROSE Collaboration). *Elsevier B.V. Nuclear Instruments and Methods in Physics Research A 439 (2000) 282-292*, 2000.

[17] Kopecky J. Atlas of Neutron Capture Cross Sections, 1997.

[18] Vasilescu A and Lindström G. Notes on the fluence normalisation based on the NIEL scaling hypothesis. *ROSE/TN/2000-02*, 2000.

[19] ASTM E722-09. Standard Practice for Characterizing Neutron Fluence Spectra in Terms of an Equivalent Monoenergetic Neutron Fluence for Radiation-Hardness Testing of Electronics. Technical report, ASTM International, West Conshohocken, PA, 2009.

[20] Lindstroem G and Vasilescu A. Displacement Damage in Silicon. `https://rd50.web.cern.ch/niel/`, 2000. [Online; accessed 27-May-2021].

[21] Lindström G. Radiation damage in silicon detectors. *Elsevier B.V. Nuclear Instruments and Methods in Physics Research A 512 (2003) 30-43*, 2003.

[22] Technische Universität Wien Atominstitut. Technische Daten ATI Reaktor. `https://ati.tuwien.ac.at/reaktor/technische_daten/`, 2019.

[23] General Atomic. *Calculated Fluxes and cross sections for Triga Reactors by G.B. West.* John Jay Hopkins Laboratory for pure and applied science P.O. Box 609, San Diego 12 California, 14 August 1963.

[24] Cognazzo M. *Neutronic modelling of the new TRIGA core and experimental validation.* PhD thesis, TU Wien.

[25] Hainz head of radiation protection ATI D. Auswertung der co-60 bestrahlungen. Private Communication.

[26] Snoj L, Zerovnik G, and Trkov A. Computational analysis of irradiation facilites at the jsi triga reactor. *Elsevier Ltd. Applied Radiation and Isotopes 70 (2012) 483-488*, 2011.

[27] *Methods in Irradiation Experiment Modelling*, Joint ICTP/IAEA Workshop.

[28] Cubdri et al. V. Measurement of the charge collection in irradiated miniature sensors for the upgrade of the ATLAS phase-ii strip tracker. *Nuclerar Inst. and Methods in Physics Research, A*, 2018.

[29] Furgeri A. *Quality Assurance and Irradiation studies on CMS silicon strip sensors.* PhD thesis, Universität Karlsruhe, 2006.

Die approbierte gedruckte Originalversion dieser Diplomarbeit ist an der TU Wien Bibliothek verfügbar
The approved original version of this thesis is available in print at TU Wien Bibliothek.
TU Bibliothek Your knowledge hub WIEN

[30] Ohsugi et al. T. Micro-discharge noise and radiation damage of silicon microstrip sensors. *Nuclear Instruments and Methods in Physics Research Section A: Accelerators, Spectrometers, Detectors and Associated Equipment*, 1996.

[31] Barney D, Guthoff M, Honma A, Li S-W, Peisert A, Tzeng Y-M, and Qin G. Measurement of the bulk leakage current of silicon sensors of the CMS Preshower after an integrated luminosity of 6.17 $fb^{-1}$, at $\sqrt{s}$ = 7 tev. *Journal of Instrumentation*, 2013.

Die approbierte gedruckte Originalversion dieser Diplomarbeit ist an der TU Wien Bibliothek verfügbar
The approved original version of this thesis is available in print at TU Wien Bibliothek.
TU Bibliothek Your knowledge hub WIEN